2011

Efficient and Robust Signal Detection Algorithms for the Communication Applications

Lu Lu
Louisiana State University and Agricultural and Mechanical College, llu4@tigers.lsu.edu

EFFICIENT AND ROBUST SIGNAL DETECTION ALGORITHMS FOR THE COMMUNICATION APPLICATIONS

A Dissertation
Submitted to the Graduate Faculty of the
Louisiana State University and
Agricultural and Mechanical College
in partial fulfillment of the
requirements for the degree of
Doctor of Philosophy

in

The Department Program in
Electrical and Computer Engineering

by
Lu Lu
B.S. Taiyuan University of Science and Technology
M.S. Xi'an Jiaotong University
December, 2011

To my parents and wife

ACKNOWLEDGMENTS

First of all, I would like to express my gratitude to my major professor and dissertation adviser-Dr. Hsiao-Chun Wu for his supervision, advice, and guidance for my Ph.D. research. His constant encouragement and precious experience really inspire this work throughout my Ph.D. studies. Without his guidance and motivation, this dissertation would not have been completed.

I am also very grateful to other faculty members in my Ph.. dissertation committee, including Dr. Jerry Trahan, Dr. Xin Li, Dr. Mark Davidson, and Dr. Rahul Shah for kindly spending their valuable time and providing me with outstanding suggestions and advice on my thesis work.

Moreover, I also want to acknowledge my laboratory mates Dr. Kun Yan, Mr. Xiaoyu Feng, Ms. Charisma Edwards, Mr. Yonas Debessu, and Ms. Hongting Zhang for their warm friendship and invaluable collaboration on research, course work, and other academics.

At last but not least, I am greatly indebted to both my parents and my wife, for their love, support, and patience during this Ph.D. research.

TABLE OF CONTENTS

ACKNOWLEDGMENTS . . . . . **ii**

LIST OF TABLES . . . . . **vi**

LIST OF FIGURES . . . . . **vii**

ABSTRACT . . . . . **ix**

1 INTRODUCTION OF DETECTION AND ESTIMATION **1**
- 1.1 Existing Solutions and Limitations 1
- 1.2 Research Motivation and Applications 4
- 1.3 Literature Review 8
  - 1.3.1 Source Localization 8
  - 1.3.2 Normality Test 10
  - 1.3.3 Spectrum Sensing 11
- 1.4 Notations 12

2 SOURCE LOCALIZATION **13**
- 2.1 Source Localization 13
  - 2.1.1 Problem Definition 14
  - 2.1.2 Maximum-Likelihood and Simplification 16
  - 2.1.3 EM Source-Localization Algorithm for Distinct Noise Variances . . . 19
- 2.2 Computational Complexities Studies and Robustness Analysis for Source Localization Algorithms 27
  - 2.2.1 Computational Complexities for Complex Multiplications 27
  - 2.2.2 Computational Complexities for Minimization 28
  - 2.2.3 Robustness Analysis for Source Localization Algorithms 29
  - 2.2.4 Conclusion 31

3 NORMALITY TEST **44**
- 3.1 Normality Test 44
  - 3.1.1 Problem Definition 45
  - 3.1.2 Kullback-Leibler Divergence Analysis 45
  - 3.1.3 Gaussian and Generalized Gaussian PDFs 47
  - 3.1.4 Skewness and Two-Sample t-Test 49
- 3.2 New KGGS Test and Its Application for Signal Detection 50
  - 3.2.1 KGGS Test 50

3.2.2 Composite Rule for Step 3 in 3.2.1 . . . 51
3.2.3 Our Proposed KGGS Test for Signal Detection . . . 54
3.2.4 Conclusion . . . 56

4 SPECTRUM SENSING . . . 59
4.1 Spectrum Sensing . . . 59
4.1.1 Problem Definition . . . 60
4.2 Efficient Spectrum Sensing Techniques . . . 62
4.2.1 Higher-Order-Statistics Spectrum-Sensing Algorithm . . . 62
4.2.2 Jarqur-Bera (JB) Statistic Based Detection Algorithm . . . 63
4.2.3 Simulation for HOS Detection and Our Proposed JB Detection . . . 69
4.3 Normality, Spectral and Computational Complexity Analysis . . . 72
4.3.1 Edgeworth Expansion for PDF Characterization . . . 73
4.3.2 Gaussianity Measure Using KGGS Test . . . 74
4.3.3 Spectral Analysis . . . 75
4.3.4 Computational Complexity Analysis . . . 77
4.3.5 Conclusion . . . 79

5 CONCLUSION . . . 89

BIBLIOGRAPHY . . . 91

APPENDIX: LETTER OF PERMISSION . . . 98

VITA . . . 101

LIST OF TABLES

3.1 Rejection Percentages for the Gaussian Hypothesis (at a 0.05 level of significance) 55

3.2 Rejection Percentages for the Gaussian Hypothesis (at a 0.05 level of significance) 55

4.1 JB Statistic Analysis 68

4.2 Rejection Rates of KGGS Normality Test 75

LIST OF FIGURES

2.1 Localization of two wide-band sources in the near field. 33

2.2 The localization of two wide-band (acoustic) sources in the near field corrupted by the noises with non-uniform variances (signal-to-noise ratio is 10 dB). The initial location estimates and the ultimate location estimates resulted from the EM algorithm (3 iterations are taken) are also demonstrated. 34

2.3 Average RMS localization errors versus SNR for the sources corrupted by the noises with non-uniform variances. The initial location estimates are plotted in Figure 2.2. 35

2.4 Average RMS localization errors versus SNR for the sources corrupted by the noises with non-uniform variances. The initial source location estimates here are randomly chosen within the areas which are one meter around the initial location estimates used in Figure 2.2. 36

2.5 The eighteen different initial source location estimates. 37

2.6 Average RMS localization errors versus SNR for the sources corrupted by the noises with non-uniform variances. The initial source location estimates are plotted in Figure 2.5. 38

2.7 Average RMS localization errors versus SNR for the sources corrupted by the noises with identical variances. The initial source location estimates are plotted in Figure 2.2. 39

2.8 Average RMS localization errors versus SNR for the sources corrupted by the noises with identical variances. The initial source location estimates are randomly drawn from the areas which are one meter around the initial source location estimates in Figure 2.2. 40

2.9 Average RMS localization errors versus SNR for the sources corrupted by the noises with identical variances. The initial source location estimates are plotted in Figure 2.5. 41

2.10 The computational complexity curves (the number of complex multiplications per iteration) versus the number of sources M for the three schemes in comparison ($\jmath = 256$ and $P = 5$). 42

2.11 Cramer-Rao lower bounds and simulated (actual) RMS localization errors versus different SNR values for the three schemes in comparison. 43

3.1 Receiver operating characteristic (ROC) curves for BPSK signal detection. Note that the confidence level for Lilliefors test can not exceed 0.2 (see [1]). . 57

3.2 Receiver operating characteristic (ROC) curves for QPSK signal detection. Note that the confidence level for Lilliefors test can not exceed 0.2 (see [1]). . 58

4.1 The topology of a wireless regional area network (WRAN). 80

4.2 The spectrum sensing system diagram. 81

4.3 A histogram example of the JB statistics. 82

4.4 False detection rate versus sample size in the sole presence of AWGN. 82

4.5 Detection rate for simulated wireless microphone signals versus SNR in the single-source case. 83

4.6 Detection rate for real DTV signals versus SNR in the single-source case. . . 83

4.7 Detection rate for real DTV signals versus SNR in the two-source case. . . . 84

4.8 The actual PDF resulting from the Edgeworth expansion and the PDF using the underlying Gaussian model for received data ($N = 30,000$, N_{FFT}=2048). 84

4.9 The actual PDF resulting from the Edgeworth expansion and the PDF using the underlying Gaussian model for received data ($N = 70,000$, N_{FFT}=2048). 85

4.10 $|R_{\text{out}}(k)|$ versus frequency $\frac{2k\pi}{N_{\text{FFT}}}$ ($N = 30,000$). 85

4.11 $|R_{\text{out}}(k)|$ versus frequency $\frac{2k\pi}{N_{\text{FFT}}}$ ($N = 70,000$). 86

4.12 Detection rate for real DTV signals versus SNR in the single-source case when the JB detector and the HOS detector are both based on the half-period feature $R_{\text{out}}(k)$, $k = 0, 1, \ldots, \frac{N_{\text{FFT}}}{2} - 1$. 87

4.13 Computational complexity measures versus N_{FFT} for our proposed JB detector and the HOS detector. 88

ABSTRACT

Signal detection and estimation has been prevalent in signal processing and communications for many years. The relevant studies deal with the processing of information-bearing signals for the purpose of information extraction. Nevertheless, new robust and efficient signal detection and estimation techniques are still in demand since there emerge more and more practical applications which rely on them. In this dissertation work, we proposed several novel signal detection schemes for wireless communications applications, such as *source localization algorithm*, *spectrum sensing method*, and *normality test*. The associated theories and practice in *robustness*, *computational complexity*, and *overall system performance evaluation* are also provided.

1. INTRODUCTION OF DETECTION AND ESTIMATION

Signal detection [2–5] and estimation [5–8] is to extract information about some phenomena related to the random observation Y, which may be a set of vectors, waveforms, numbers, and so on. The *detection* problem is to decide among a finite number of possible situations or "states of nature", and the *estimation* problem is to estimate the values of some *parameters* that cannot be observed directly. In either case, the relation between the observation and the desired information is probabilistic rather than deterministic, in the sense that the statistical behavior of Y is affected by the states of nature or the values of the parameters to be estimated. Thus, the corresponding mathematical model involves a family of probability distributions of Y. Given such a statistical model, the detection and estimation problems are to find the optimal approaches to process the observation Y in order to extract the desired information. The differences in the fundamental attributes of these approaches can be reflected by the characteristics of the desired information, the amount of *a priori* knowledge, and the associated objective measures [8].

1.1 Existing Solutions and Limitations

There exist many different kinds of signal detection and estimation applications and techniques [4, 7, 9–13]. The binary- and multiple-hypothesis tests, for example, Bayesian and Neyman-Pearson (NP) tests, are widely used [14, 15]. For the binary-hypothesis tests, the

optimal decision rules can be expressed in terms of *likelihood ratio* (LR) statistics and the test performances can be analyzed using the *receiver operating characteristic* (ROC). However, one may ask how to make sure that those decisions are subject to a high degree of reliability. In the signal detection, two different strategies can often be employed to reach the *highly reliable decisions*. The first strategy is to mandate the signal detector to operate at a sufficiently high signal-to-noise ratio (SNR). But this is not always possible. The second strategy is to repeatedly acquire measurements until the reliability of the decision is attained. Thus, the tests based on repeated measurements are developed for the second strategy.

For all the aforementioned detection techniques, the probability distributions of observations under all hypotheses are known exactly. However, this assumption is not true in practice; either the probability distribution functions cannot be characterized precisely or there exist some unknown parameters associated with the underlying probability density function, which depend on the observations. The estimation of unknown parameters from observations depends on whether the unknown parameters are deemed random or deterministic. Different methods can be devised to facilitate the estimates. Bayesian methods in [14] treat these parameters random but with a known *a priori* probability distribution. This distribution can be acquired from long-term measurements or presumption. The minimum mean-square error (MMSE) and maximum *a posteriori* (MAP) estimators are two commonly used Bayesian approaches [14, 16]. On the other hand, the deterministic approach treats the unknown parameters deterministic and relies exclusively on the available data. The best-known deterministic method is the *maximum likelihood* (ML) *estimator* which maximizes the probability density function of the observations subject to the unknown parameters. Usually, the ML estimate converges almost surely to the true parameter value, but the corresponding com-

putational complexity is increased with the sample size [11].

In addition, Gaussian signal detection is one of the most important signal detection problems because the Gaussian model is prevalent in all practical applications. Often, it can be found that a received signal is assumed deterministic possibly involving some unknown parameters, and it is impaired by Gaussian noise. A typical example can be found in the detection of the received M-ary *phase-shift keying* (PSK) or *frequency-shift-keying* (FSK) signals [17]. Besides, a received signal itself may constitute a Gaussian process involving some unknown parameters [11]. Dependent on the type of applications, usually a *Bayesian test* or a *generalized likelihood ratio test* (GLRT) can be adopted for the Gaussian signal detection [18]. To detect such Gaussian signals [11], one needs to undertake a GLRT detector incorporated with the ML estimators [19] and the unknown parameters can be determined thereby. This task can be undertaken using standard iterative methods, such as *Gauss-Newton iteration* [20]. However, among all iterative techniques, the *expectation-maximization* (EM) algorithm facilitates a convenient approach to simplify the maximum likelihood [21]. Whenever the solution of the maximum likelihood cannot be achieved in a closed form, the available observations should be augmented by "missing data" until the "complete data" constituting both observations and missing data lead to a new solvable maximum likelihood. Since the missing data are unavailable, they need to be estimated at each iteration. Consequently, the EM algorithm proceeds by two steps: in the expectation step (E-step), the missing data are estimated using the available data (observations) subject to the current estimates of the unknown parameters; in the maximization step (M-step), the estimated likelihood function subject to the complete data is then maximized so as to obtain a set of updated parameters. In conclusion, for different applications and problems, different signal detection and esti-

mation methods need to be used. Before designing an appropriate approach to solve any problem, one needs to answer the two following questions.

- Given a particular application or problem, how do we extract the "best" features from the observations?
- Given a particular application or problem, how do we design a "robust" and "efficient" algorithm to solve it?

Since the answers to the two aforementioned questions are surely application- or problem-dependent, many on-going research works are still in pursuit in the scientific society nowadays [22–25]. In this dissertation work, we would also like to dedicate our point of view in dealing with the relevant detection/estimation problems.

1.2 Research Motivation and Applications

Based on our previous discussion, it is obvious that the most important issue in signal detection and estimation is to find the "reliable features" which can represent the "crucial" statistical information of all observations (signals), and also to develop the robust statistical methods, tests, or algorithms to extract/estimate these features. There exist many signal detection and estimation techniques nowadays. However, because more and more new applications emerge in signal processing and communications, researchers are still making continual efforts to design novel robust statistical methodologies for signal detection and estimation. Thus, we will dedicate this dissertation work to exploring the robust statistical features and the associated computationally-efficient detection and/or estimation algorithms for some focused applications.

Among a wide variety of statistical features, probability density function (PDF) is one of the most important features, since PDF is the only complete mathematical representation for any random process. By simply maximizing the PDF with respect to the unknown parameters, one can carry out the estimation or detection. This general inference procedure is the well-known *maximum likelihood method*. In order to deal with noise and determine a reliable analytical statistical model of the signal, Gaussian distribution is commonly adopted for signal detection or estimation. Based on the central limit theorem [26], most noises could be modeled as Gaussian processes in practice. Nevertheless, Gaussian distribution is not a simple polynomial function. Thus, the analytical statistical model for the signal based on the Gaussian distribution is usually not mathematically tractable. Moreover, the maximum likelihood problem is generally quite complicated. For example, when the underlying PDF is assumed to be a Gaussian mixture, the corresponding optimization solution will not be easy to obtain. Thus, robust and efficient iterative algorithms need to be designed to approximate the optimal solution step by step [27]. On the other hand, though the Gaussian model is a nominal assumption which may often be valid, it turns out that in many cases the optimal signal processing schemes can still suffer a drastic degradation in performance even for apparently small deviations from such a nominal assumption. Thus, other types of PDFs, such as Rayleigh distribution, Gamma distribution, etc. [28], were also employed to facilitate the statistic features of the signals in practice. One can discover that based on different PDFs, one needs to employ different statistical methods to fully extract the reliable information of the signal. Thus, above all, one has to make sure whether the observations satisfy a specific distribution. Since the Gaussian model is the most commonly used statistical model, it would be very desirable to check whether the observation data satisfy a Gaussian distribution or

not before any detection or estimation task is carried out.

To demonstrate our proposed signal detection/estimation schemes, three practical problems (applications) will be illustrated as typical examples in this dissertation, namely *source localization*, *normality test*, and *spectrum sensing*. These three applications are briefly introduced as follows.

- Source Localization: Source localization problem is to target the locations of the sources using the collected data at low-cost and low-complexity passive sensor arrays, which are transmitted from the sources. This has been the underlying problem in radar, sonar, wireless systems, radio-astronomy, seismology, and many other applications for long.

- Normality Test: It is well known that Gaussian PDF is the widely adopted underlying statistical model due to the central limit theorem and this statistical model has been exhaustively used in all engineering and science applications. Desirable mathematical properties can be found subject to the underlying Gaussian PDF. However, before adopting the Gaussian model for some arbitrary observations, one needs to determine if such observations satisfy the Gaussian distribution. This decision-making task is called *Gaussianity* (*normality*) *test*, which is essential for many signal processing applications [29–33].

- Spectrum Sensing: The increasing demand for wireless connectivity and the crowded unlicensed spectra have prompted the regulatory agencies to be more aggressive in coming up with new ways to use spectra more wisely [34]. Hence, *spectrum sensing* (see [35, 36]) arises as a feasible solution to the aforementioned spectral congestion

problem by introducing the opportunistic usage of the frequency bands that are not heavily occupied by licensed users [37, 38].

When the iterative algorithms are employed for detection or estimation, one must consider how fast they can converge or whether they would be easy to be trapped into local minima/maxima [39, 40]. For some methods, their convergence can be analyzed by rigorous mathematical manipulations, while for other algorithms, they are not mathematically tractable. Thus, for those iterative algorithms whose convergence can only be empirically justified, one needs to undertake sufficiently many random tests to investigate their convergence behaviors. Computational complexity is another important factor, and it depends on the required sample size and iteration number, and so on.

The "robustness" factor is also very important for researchers in designing any detection or estimation method. The "robust techniques" (techniques leading to a satisfactory performance even if there involves some uncertainty in the assumption of the system model) will help us get much more reliable results in practice. Moreover, the detection/estimation methods must be efficient as well. In this dissertation work, we will explore novel detection/estimation methods which are both robust and efficient.

To measure the performance of a detection or estimation technique, *Cramer-Rao lower bounds* (CRLBs) and ROCs are often used. By comparing the CRLBs or ROCs, one can easily determine which method is superior. On the other hand, *Monte Carlo* (MC) simulations should be investigated as well. Together with CRLB/ROC analysis and MC simulation results, one can evaluate and compare the performances of different estimation or detection methods.

1.3 Literature Review

Signal detection and estimation theory is based on mathematical statistics. Fundamental monographs written by A. Kolmogorow, V. Kotellnikow, N. Wiener, and K. Shannon explored the techniques of statistics for signal processing in general and for detection and estimation in particular [41–43]. The first fundamental research devoted to the systematic use of statistics for solving the problems of signal detection and estimation was carried out by J. Marcum, P. Swerling, and V. Kotelnikow [41, 42]. Many results of fundamental importance were presented by these authors. Much of the early work in detection and estimation theory was undertaken by radar researchers [44]. Moreover, signal detection and estimation theory was applied in 1966 by John A. Swets and David M. Green for psychophysics [45]. Nowadays, signal detection and estimation theory is used in many different areas, especially telecommunications. The basic knowledge about signal detection and estimation can be found in the existing literature [5, 9, 11, 26, 28, 46–48].

1.3.1 Source Localization

Recently, the wide-band source localization in the near field has drawn a lot of research interest in the signal processing applications [49–52]. Extensive studies for the wide-band source localization can be found in [49, 50]. Among them, the maximum-likelihood (ML) approach in [49] has been regarded as the optimal and robust scheme for coherent source signals. However, when multiple sources are present, the ML approach facilitates a nonlinear optimization problem, which is impractical especially for the energy-constrained sensor networks. In addition, many of the existing ML estimators are based on the unrealistic

spatially-white noise assumption across different sensors [51–53], where the noise process at each sensor is assumed to be spatially-uncorrelated-white-Gaussian with an identical variance. It is shown that under this assumption, the ML estimates of the unknown parameters (source waveforms/spectra and noise variance) can be expressed as the respective functions of the source locations and the number of independent parameters to be estimated is greatly reduced. Thus, this assumption, although unrealistic, substantially reduces the search space and usually leads to more efficient localization algorithms. Hence, various wide-band ML source location estimators were proposed in [49]. However, this spatially-white noise assumption is unrealistic in many applications. In several practical applications [53], the sensors are sparsely placed so that the sensor noise processes are spatially uncorrelated. However, the noise variance of each sensor can still be quite different due to either the variation of the manufacturing process, the imperfection of the sensor array calibration or the "unquiet" background. As a result, the spatial noise covariance matrix (across the sensors) can be modeled as a diagonal matrix where the diagonal elements in general are not identical. Note that this noise model is definitely not a special case of the ARMA model as was explained in [54]. Furthermore, the source location estimators derived from the spatially-white noise (SWN) assumption would often not provide satisfactory results in the real environment since the algorithms derived from the SWN assumption blindly treat all sensors equally in the estimated likelihood. Motivated by the arguments above, a narrow-band ML DOA (direction of arrival) estimator under the realistic spatially-non-white noise (SNWN) model has been recently proposed [54]. In [53], two DOA calculation algorithms, namely *stepwise-concentrated maximum likelihood estimator* (SC-ML) and *approximately-concentrated maximum likelihood algorithm* (AC-ML), were presented for the multiple wide-band sources instead. Although

both SC-ML and AC-ML methods can be extended for the source localization, the robustness issue still remain challenging in this research area.

1.3.2 Normality Test

For the time-domain approach, the existing techniques are summarized as follows. The classical *goodness-of-fit* tests based on the χ^2 or Kolmogorov-Smirnov statistic can be employed to verify the Gaussianity [55]. The most commonly-used technique is the Pearson's χ^2 test. Other popular tests include the Shapiro-Wilk test in [56] and the D'Agostino test in [57]. In addition, the Lilliefors test in [58] is a special case of the Kolmogorov-Smirnov goodness-of-fit test. In the Lilliefors test, the Kolmogorov-Smirnov test is implemented using the sample mean and the standard deviation as the mean and the standard deviation of the theoretical (benchmark) population with which the observed sample is compared. Jarque-Bera (JB) test in [59] based on the sample kurtosis and the sample skewness is very promising. The JB statistic used in this method has an asymptotic chi-square distribution with two degrees of freedom. In this test, the null hypothesis is that the data consist of a normal (Gaussian) distribution. This null hypothesis is a joint hypothesis of both skewness and excess kurtosis being zero, since a Gaussian process has an expected skewness of 0 and an expected excess kurtosis of 0 (or a kurtosis of 3). As shown in [59], any deviation from the Gaussianity increases the JB statistic. Moreover, some statistical tests based on the characteristic functions were proposed in [60] and they usually required the estimation of much more parameters than the aforementioned simple tests. On the other hand, the main frequency-domain Gaussianity test was originally proposed by Hinich, which was based on the bispectrum. Although Hinich's bispectrum test drew many applications, it is not suit-

able for the symmetric PDFs [61]. This test was later extended to the trispectrum based technique by [62]. Both bispectrum and trispectrum based statistics have the nonparametric advantage. However, a large amount of data are required for reliable spectral estimates and the additional time-consuming bootstrap technique may also often be in demand [61].

1.3.3 Spectrum Sensing

To combat the spectrum sensing problem, several methods have been proposed, such as the matched filtering approach [34, 63, 64], the feature detection approach [65, 66] and the energy detection approach [63, 67–70]. For the matched filtering method, it can maximize the SNR inherently. However it is difficult to do detection without signal information such as pilot and frame structure. And for feature detection method which is basically performed based on cyclostationarity, it also must have information about received signal sufficiently. However, in practice, cognitive radio system can not know about primary signals structure and information. For the energy detection method, although it doesn't need any information about the signal to be detected, it is prone to false detections since it is only based on the signal power [69, 70]. When the signal is heavily fluctuated or noise uncertainty is big [63,64,69], it becomes difficult to discriminate between the absence and the presence of the signal. In addition, the energy detection is not optimal for detecting the correlated (colored) signals, which are often found in practice. To overcome the shortcomings of the energy detection approach, some methods based on the eigenvalues associated with the covariance matrix of the received signal were proposed in [37, 71, 72]. However, the corresponding computational complexities are quite large. A method based on the higher-order-statistics (HOS) was proposed and it would be promising especially in the low SNR conditions [73].

1.4 Notations

The sets of all real and complex numbers are denoted by $\mathcal{R}$ and $\mathcal{C}$, respectively. A vector is denoted by $\underline{A}$ and a matrix is denoted by $\widetilde{A}$. The statistical expectation operation is expressed as $\mathbb{E}\{\ \}$. Besides, $\widetilde{A}^T$, $\widetilde{A}^*$, $\widetilde{A}^H$, $\det(\widetilde{A})$, $\widetilde{A}^\dagger$, and $\text{trace}(\widetilde{A})$ stand for the transpose, conjugate, Hermitian adjoint, determinant, pseudo-inverse, and trace of the matrix $\widetilde{A}$, respectively. In addition, $\odot$ stands for the Hadamard matrix product operator, and $\|\ \|$ stands for the Euclidean norm.

2. SOURCE LOCALIZATION[1]

In this chapter, we would like to discuss the source localization problem. Weak signal detection is the crucial challenge in source localization applications. Besides, the realistic scenario that the source signal waveform is unknown would impose difficulty to source localization as well. Hence, the robustness against sparse weak signals and the efficiency of the relevant methods will be investigated in this dissertation work.

2.1 Source Localization

Figure 2.1 illustrates a simple example of source localization. Two acoustic sources and five sensors (receivers) are placed in a given territory. Based on the PDFs of the received data at each sensor, the locations of the two sources could be estimated using the ML approach. This chapter is organized as follows. The problem formulation and the signal model are introduced in Section 2.1.1. The maximum-likelihood source-location estimators for both SWN and SNWN models are introduced in Section 2.1.2. The novel EM algorithm for

[1] © [2011] IEEE. Reprinted, with permission, from [Lu Lu, Hsiao-Chun Wu, Kun Yan, and Iyengar, S.S., "Robust Expectation-Maximization Algorithm for Multiple Wideband Acoustic Source Localization in the Presence of Nonuniform Noise Variances", IEEE Sensors Journal, March/2011].

wide-band source localization in the near field under the SNWN assumption is derived and discussed in Section 2.1.3. Then the computational complexity comparison among our new EM algorithm, the conventional SC-ML and AC-ML methods is presented in Sections 2.2.1 and 2.2.2. In addition, the Cramer-Rao lower bound (CRLB) derivation will be manifested in Section 2.2.3. Conclusion will be drawn in Section 2.2.4.

2.1.1 Problem Definition

Considering a randomly distributed array of P sensors to collect the data from M sources, we assume a problem structure illustrated in Figure 2.1. Since the sources are assumed to be in the near field, the signal gains are different across the sensors. Thus, the signal collected by the p^{th} sensor at a discrete time instant $\imath$ is given by

$$æ_p(\imath) = \sum_{m=1}^{M} a_p^{(m)} s^{(m)}\left(\imath - \varrho_p^{(m)}\right) + w_p(\imath), \tag{2.1}$$

for $\imath = 0, 1, \ldots, L-1$, $p = 1, \ldots, P$, $m = 1, \ldots, M$, where $a_p^{(m)}$ is the gain of the m^{th} source signal arriving at the p^{th} sensor; $s^{(m)}(\imath)$ denotes the m^{th} source signal waveform; $\varrho_p^{(m)}$ is the propagation delay (in data samples) incurred from the m^{th} source to the p^{th} sensor; $w_p(\imath)$ represents the zero-mean independently identically distributed (i.i.d.) noise process. Several crucial parameters are specified as follows:

$\varrho_p^{(m)} \overset{\text{def}}{=} F_s \frac{\left\|\underline{r_s}^{(m)} - \underline{r_p}\right\|}{v}$: the propagation delay from the m^{th} source to the p^{th} sensor,

$\underline{r_s}^{(m)} \in \mathcal{R}^{2\times 1}$: the m^{th} source location,

$\underline{r_p} \in \mathcal{R}^{2\times 1}$: the p^{th} sensor location,

v: the source signal propagation speed in meters/second,

F_s: sampling frequency.

Taking the $\jmath$-point discrete Fourier transform (DFT) of both sides in Eq. (2.1) and reserving a half of them due to the symmetry property, we have

$$\underline{X}(k) = \widetilde{D}(k)\underline{S}(k) + \underline{U}(k), \quad \text{for} \quad k = 0, 1, \ldots, \frac{\jmath}{2} - 1, \tag{2.2}$$

where

$$\underline{X}(k) \stackrel{\text{def}}{=} [X_1(k), \ \cdots \ , X_P(k)]^T \in \mathcal{C}^{P\times 1} \tag{2.3}$$

and $X_p(k)$ is the k^{th} DFT point of $x_p(n)$, $p = 1, \ldots, P$. The symbols for the right-hand side of Eq. (2.2) are clarified as follows.

$$\widetilde{D}(k) \stackrel{\text{def}}{=} [\underline{d}^{(1)}(k), \ \cdots \ , \underline{d}^{(M)}(k)] \in \mathcal{C}^{P\times M} \tag{2.4}$$

consists of M *steering vectors*, each given by

$$\underline{d}^{(m)}(k) \stackrel{\text{def}}{=} [d_1^{(m)}(k), \ \cdots \ , d_P^{(m)}(k)]^T \in \mathcal{C}^{P\times 1}, \ \ m = 1, \ldots, M, \tag{2.5}$$

where

$$d_p^{(m)}(k) \stackrel{\text{def}}{=} a_p^{(m)} e^{-\frac{\jmath 2\pi k t_p^{(m)}}{\jmath}}, \tag{2.6}$$

and $\jmath \stackrel{\text{def}}{=} \sqrt{-1}$. Note that

$$\underline{S}(k) \stackrel{\text{def}}{=} [S^{(1)}(k), \ \cdots \ , S^{(M)}(k)]^T \in \mathcal{C}^{M\times 1} \tag{2.7}$$

consists of M individual source signal spectra, each given by $S^{(m)}(k)$ where $S^{(m)}(k)$ is the k^{th} DFT point of $s^{(m)}(n)$, $m = 1, \ldots, M$.

In reality, the source signal spectral vector $\underline{S}(k)$ is unknown and deterministic. The noise spectral vector $\underline{U}(k) \in \mathcal{C}^{P\times 1}$ is a complex-valued zero-mean spatially-uncorrelated Gaussian process with the following covariance matrix:

$$\widetilde{Q} \stackrel{\text{def}}{=} \mathbb{E}\left\{\underline{U}(k)\,\underline{U}(k)^H\right\} = \begin{bmatrix} q_1 & 0 & \cdots & 0 \\ 0 & q_2 & \ddots & \vdots \\ \vdots & \ddots & \ddots & 0 \\ 0 & \cdots & 0 & q_P \end{bmatrix} \in \mathcal{C}^{P\times P}, \forall k. \tag{2.8}$$

In general, q_p, $p = 1, 2, \ldots, P$, are not necessarily identical to each other under the SNWN assumption. Hence, we need to deal with the realistic source localization problem in the presence of the non-uniform noise variances thereupon.

2.1.2 Maximum-Likelihood and Simplification

Prior to the establishment of the log-likelihood for the source localization in the presence of the non-uniform noise variances as stated by Eq. (2.8), we start from the conventional maximum-likelihood formulation for the identical noise variance across the sensors.

Conventional Maximum-Likelihood for Source Localization in the Presence of Identical Noise Variance (SWN)

According to the signal model given by Eq. (2.2) together with the noise variance constraint as $\widetilde{Q} = \sigma^2\,\widetilde{I}$, where σ^2 is the noise variance and $\widetilde{I}$ is a $P \times P$ identity matrix, the maximum-likelihood source localization formulation can be facilitated as [49, 53, 74]. We highlight the relevant pivotal formulae here.

Let $\underline{r_s}$, $\widetilde{S}$, σ^2 represent all the unknown parameters in Eq. (2.2) necessary to be estimated, where

$$\underline{r_s} \stackrel{\text{def}}{=} \left[\underline{r_s}^{(1)^T},\ \cdots,\underline{r_s}^{(m)^T},\ \cdots,\underline{r_s}^{(M)^T}\right]^T \in \mathcal{R}^{2M\times 1}, \tag{2.9}$$

$$\widetilde{S} \stackrel{\text{def}}{=} \left[\underline{S}(0)^T, \ \cdots \ , \underline{S}\left(\jmath/2-1\right)^T\right]^T \in \mathcal{C}^{\left(\frac{M\jmath}{2}\right)\times 1}. \tag{2.10}$$

In addition, we denote the *residual vector* as

$$\underline{g}(k) \stackrel{\text{def}}{=} [g_1(k), \ \cdots \ , g_P(k)]^T = \underline{X}(k) - \widetilde{D}(k)\underline{S}(k) \in \mathcal{C}^{P\times 1}. \tag{2.11}$$

Thus, the likelihood function is given by

$$f(\underline{r_s}, \widetilde{S}, \sigma^2) \stackrel{\text{def}}{=} \frac{1}{\pi^{P\jmath/2}\sigma^{P\jmath}} \exp\left\{-\frac{1}{\sigma^2}\sum_{k=0}^{\jmath/2-1}\left\|\underline{g}(k)\right\|^2\right\}. \tag{2.12}$$

Taking the logarithm of Eq. (2.12) and neglecting all the constant terms, we can derive the corresponding maximum likelihood estimates are

$$\left(\widehat{\underline{r_s}}, \widehat{\widetilde{S}}, \widehat{\sigma^2}\right) \ = \ \underset{\left(\underline{r_s},\widetilde{S},\sigma^2\right)}{\arg\max}\left\{L\left(\underline{r_s}, \widetilde{S}, \sigma^2\right)\right\} = \underset{\left(\underline{r_s},\widetilde{S},\sigma^2\right)}{\arg\min}\left(\sum_{k=0}^{\jmath/2-1}\left\|\underline{g}(k)\right\|^2\right). \tag{2.13}$$

Thus, according to Eq. (2.13), we can write

$$\widehat{\underline{S}}(k) = \widetilde{D}(k)^{\dagger}\underline{X}(k) = \left(\widetilde{D}(k)^H\widetilde{D}(k)\right)^{-1}\widetilde{D}(k)^H\underline{X}(k), \tag{2.14}$$

and

$$\widehat{\underline{r_s}} = \underset{\underline{r_s}}{\arg\min}\sum_{k=0}^{\jmath/2-1}\left\|\underline{X}(k) - \widetilde{D}(k)^{\dagger}\underline{X}(k)\right\|^2. \tag{2.15}$$

Maximum-Likelihood for Source Localization in the Presence of Non-uniform Noise Variances (SNWN)

In this subsection, we will introduce the nonuniform maximum-likelihood source localization formulation according to the recent literature [53, 54] for a more realistic SNWN model. Let $\underline{r_s}$, $\widetilde{S}$, $\underline{q}$ be the parameters to be estimated for this case, where $\underline{q} \stackrel{\text{def}}{=} [q_1, ..., q_P]^T \in \mathcal{R}^{P\times 1}$ is the vector consisting of the diagonal elements in $\widetilde{Q}$ given by Eq. (2.8). The likelihood function of $\left(\underline{r_s}, \widetilde{S}, \underline{q}\right)$ can be expressed as

$$f\left(\underline{r_s}, \widetilde{S}, \underline{q}\right) \stackrel{\text{def}}{=} \frac{1}{\left(\pi^p \det(\widetilde{Q})\right)^{\jmath/2}} \exp\left\{-\sum_{k=0}^{\jmath/2-1} \underline{g}(k)^H \widetilde{Q}^{-1} \underline{g}(k)\right\}. \tag{2.16}$$

Then we have the following log-likelihood function $L\left(\underline{r_s}, \widetilde{S}, \underline{q}\right)$ by taking the logarithm of Eq. (2.16) and neglecting all the constant terms:

$$L\left(\underline{r_s}, \widetilde{S}, \underline{q}\right) = -\frac{\jmath}{2} \sum_{p=1}^{P} \log\left(q_p\right) - \sum_{k=0}^{\jmath/2-1} \left\|\underline{\dot{g}}(k)\right\|^2, \tag{2.17}$$

where

$$\underline{\dot{g}}(k) \stackrel{\text{def}}{=} \widetilde{Q}^{-1/2} \underline{g}(k) = \underline{\dot{X}}(k) - \widetilde{\dot{D}}(k) \underline{S}(k), \tag{2.18}$$

$$\underline{\dot{X}}(k) \stackrel{\text{def}}{=} \widetilde{Q}^{-1/2} \underline{X}(k), \tag{2.19}$$

$$\widetilde{\dot{D}}(k) \stackrel{\text{def}}{=} \widetilde{Q}^{-1/2} \widetilde{D}(k). \tag{2.20}$$

Consequently, we may obtain the maximum-likelihood estimates for $\left(\underline{r_s}, \widetilde{S}, \underline{q}\right)$ as

$$\left(\widehat{\underline{r_s}}, \widehat{\widetilde{S}}, \widehat{\underline{q}}\right) = \arg\max_{\left(\underline{r_s}, \widetilde{S}, \underline{q}\right)} L\left(\underline{r_s}, \widetilde{S}, \underline{q}\right). \tag{2.21}$$

Similar to the derivation in Section 2.1.2, we can obtain the estimate of the p^{th} element in $\underline{q}$ as

$$\widehat{q_p} = \frac{2}{\jmath} \sum_{k=0}^{\jmath/2-1} \left|g_p(k)\right|^2 = \frac{2}{\jmath} \left\|\underline{g_p}\right\|^2 \tag{2.22}$$

where $g_p(k)$ denotes the p^{th} element of the residual vector $\underline{g}(k)$ and

$$\underline{g_p} \stackrel{\text{def}}{=} \left[g_p(0), \ \cdots \ , g_p\left(\frac{\jmath}{2} - 1\right)\right]^T \in \mathcal{C}^{\jmath/2 \times 1}. \tag{2.23}$$

Substituting Eqs. (2.23), (2.22) into Eq. (2.16), we can convert the log-likelihood function to a new version in terms of $\underline{r_s}$ and $\widetilde{S}$ only as

$$
\begin{aligned}
L(\underline{r}_s, \widetilde{S}) &= -\frac{J}{2}\sum_{p=1}^{P}\log\left(\widehat{q}_p\right) - \sum_{k=0}^{J/2-1}\sum_{p=1}^{P}\frac{\left|g_p(k)\right|^2}{\widehat{q}_p} \\
&= \frac{J}{2}\left\{P\left[\log\left(\frac{J}{2}\right)-1\right] - \sum_{p=1}^{P}\log\left\|\underline{g}_p\right\|^2\right\}. \qquad (2.24)
\end{aligned}
$$

Thus, the ML estimators for $\underline{r}_s$ and $\widetilde{S}$ are given by

$$
\left(\widehat{\underline{r}}_s, \widehat{\widetilde{S}}\right) = \underset{\left(\underline{r}_s, \widetilde{S}\right)}{\arg\max}\left(-\sum_{p=1}^{P}\log\left\|\underline{g}_p\right\|^2\right), \qquad (2.25)
$$

and

$$
\widehat{\underline{S}}(k) = \widetilde{\dot{D}}(k)^{\dagger}\widetilde{\dot{X}}(k). \qquad (2.26)
$$

Substituting Eq. (2.26) into Eq. (2.25), we can obtain the maximum-likelihood estimates of $\underline{r}_s$ and $\underline{q}$ as

$$
\left(\widehat{\underline{r}_s}, \widehat{\underline{q}}\right) = \underset{\left(\underline{r}_s, \underline{q}\right)}{\arg\max}\, L\left(\underline{r}_s, \underline{q}\right) \qquad (2.27)
$$

where

$$
L\left(\underline{r}_s, \underline{q}\right) = -\sum_{p=1}^{P}\log\left\|\underline{g}_p\right\|^2, \qquad (2.28)
$$

$\underline{g}_p$ is defined by Eq. (2.23), and

$$
\underline{g}(k) = \underline{X}(k) - \widetilde{D}(k)\widetilde{\dot{D}}(k)^{\dagger}\widetilde{\dot{X}}(k). \qquad (2.29)
$$

2.1.3 EM Source-Localization Algorithm for Distinct Noise Variances

Individual Likelihood Formulation for Source Localization

The EM algorithm is a well-known iterative algorithm for the maximum-likelihood estimation. The complicated nonlinear optimization problem in Eq. (2.21) and Eq. (2.27) can be

simplified using the EM procedure incorporated with the *augmented (complete) data* corresponding to the individual incident source signals. First, we denote the received signal spectrum as $X_p^{(m)}(k), 1 \le p \le P, 1 \le m \le M, 0 \le k \le \jmath - 1$ from the m^{th} source to the p^{th} sensor. Then we define the augmented data as $\left\{\underline{X}^{(m)}(k); 1 \le m \le M, 0 \le k \le \jmath - 1\right\}$ where $\underline{X}^{(m)}(k) \stackrel{\text{def}}{=} \left[X_1^{(m)}(k), \ldots, X_P^{(m)}(k)\right]^T \in \mathcal{C}^{P\times 1}$.

In addition, the relationship between the observed (incomplete) data $\underline{X}(k)$ and the complete data is established as

$$\underline{X}(k) = \sum_{m=1}^{M} \underline{X}^{(m)}(k). \tag{2.30}$$

According to Eqs. (2.2), (2.5), (2.7) and (2.30), for a single source signal (the m^{th} source), we have

$$\underline{X}^{(m)}(k) \stackrel{\text{def}}{=} \underline{d}^{(m)}(k) S^{(m)}(k) + \underline{U}^{(m)}(k), \text{ for } k = 0, 1, \ldots, \jmath/2 - 1, \tag{2.31}$$

where $\underline{U}^{(m)}(k) \in \mathcal{C}^{P\times 1}$ is the complex-valued zero-mean uncorrelated Gaussian noise in the sole presence of the m^{th} source.

According to Eqs. (2.21), (2.27), (2.31), we have

$$\left(\widehat{\underline{r}_s}^{(m)}, \widehat{\underline{S}}^{(m)}, \widehat{\underline{q}}^{(m)}\right) = \underset{\left(\underline{r_s}^{(m)}, \underline{S}^{(m)}, \underline{q}^{(m)}\right)}{\arg\max} L\left(\underline{r_s}^{(m)}, \underline{S}^{(m)}, \underline{q}^{(m)}\right), 1 \le m \le M, \tag{2.32}$$

where $\underline{S}^{(m)} \stackrel{\text{def}}{=} [S^{(m)}(0) \ \cdots \ S^{(m)}(\jmath/2-1)]^T \in \mathcal{C}^{\jmath/2\times 1}$ and $\underline{q}^{(m)} \stackrel{\text{def}}{=} \left[q_1^{(m)}, ..., q_P^{(m)}\right]^T \in \mathcal{C}^{P\times 1}$ is the vector consisting of the diagonal elements in $\widetilde{Q}^{(m)} \stackrel{\text{def}}{=} \mathbb{E}\left\{\underline{U}^{(m)}(k)\left(\underline{U}^{(m)}(k)\right)^H\right\} \in \mathcal{C}^{P\times P}$, $\forall k$. Let

$$\underline{\dot{d}}^{(m)}(k) \stackrel{\text{def}}{=} \left(\widetilde{Q}^{(m)}\right)^{-1/2} \underline{d}^{(m)}(k), \tag{2.33}$$

and also let

$$\underline{\dot{X}}^{(m)}(k) \stackrel{\text{def}}{=} \left(\widetilde{Q}^{(m)}\right)^{-1/2} \underline{X}^{(m)}(k). \tag{2.34}$$

According to Eq. (2.23), we denote the p^{th} element of the particular residual vector $\underline{g}^{(m)}(k)$ as $g_p^{(m)}(k)$ when only source m is present, where

$$\underline{g}^{(m)}(k) = \underline{X}^{(m)}(k) - \underline{\dot{d}}^{(m)}(k)\, \underline{\dot{d}}^{(m)}(k)^{\dagger}\, \underline{\dot{X}}^{(m)}(k). \tag{2.35}$$

Similar to the derivation in Section 2.1.2, Eq. (2.32) yields

$$\widehat{q}_p^{(m)} = \frac{2}{\jmath} \sum_{k=0}^{\jmath/2-1} \left| \left[g_p^{(m)}(k) \right] \right|^2 = \frac{2}{\jmath} \left\| \underline{g_p}^{(m)} \right\|^2, \tag{2.36}$$

where

$$\underline{g_p}^{(m)} \stackrel{\text{def}}{=} \left[g_p^{(m)}(0),\ \cdots,\ g_p^{(m)}(\jmath/2-1) \right]^T \in \mathcal{C}^{\jmath/2 \times 1}. \tag{2.37}$$

Consequently, the maximum-likelihood estimates $\underline{\widehat{r}_s}^{(m)}$, $\underline{\widehat{q}}^{(m)}$ are given by

$$\left(\underline{\widehat{r}_s}^{(m)}, \underline{\widehat{q}}^{(m)} \right) = \underset{\left(\underline{r_s}^{(m)}, \underline{q}^{(m)} \right)}{\arg\max}\ L(\underline{r_s}^{(m)}, \underline{q}^{(m)}), \tag{2.38}$$

where

$$L\left(\underline{r_s}^{(m)}, \underline{q}^{(m)} \right) = -\sum_{p=1}^{P} \log \left(\left\| \underline{g_p}^{(m)} \right\|^2 \right). \tag{2.39}$$

According to Eqs. (2.38) and (2.39), the source localization problem can be formulated as the independent maximization sub-problems with respect to the individual likelihood functions in each iteration. Note that the log-likelihood for the source localization problem stated by Eqs. (2.32)-(2.39) can be carried out for different sources m in each iteration. In other words, we can carry out the maximum likelihood independently and separately for each individual source m in each iteration. Hence the computationally efficient techniques based on the parallel paradigm can be used in our proposed scheme especially for many sources.

New Expectation-Maximization Algorithm for Source Localization

In contrast to other existing algorithms for the source localization using the sensor signals in the presence of noises with identical variance [49,74–76], we present a new EM algorithm here to solve the realistic source localization problem for sensor signals in the presence of noises with different variances, which has been tackled by [53] recently. Nevertheless, our proposed EM algorithm can be demonstrated to be more robust and more computationally-efficient than the method proposed by [53].

The details of our proposed EM algorithm are introduced as follows (since our proposed algorithm can be decoupled across different sources, we only need to address the steps for the source m and it can be run for other sources as well in parallel in each iteration):

Initialization:

Randomly initialize $[\underline{\widehat{r}_s}^{(m)}]^{[0]}$. Set the initial values for the entries in $[\underline{\widehat{q}}^{(m)}]^{[0]}$ and $[\underline{\widehat{q}}]^{[0]}$ as

$$[\underline{\widehat{q}}^{(m)}]^{[0]} = \frac{1}{M} \times [1 \ 1 \ \cdots \ 1]^T \in \mathcal{R}^{P \times 1} \tag{2.40}$$

and

$$[\underline{\widehat{q}}]^{[0]} = [1 \ 1 \ \cdots \ 1]^T \in \mathcal{R}^{P \times 1}, \tag{2.41}$$

respectively.

Input (Given) Parameters at Iteration i: $[\underline{\widehat{q}}^{(m)}]^{[i-1]}$, $[\underline{\widehat{r}_s}^{(m)}]^{[i-1]}$.

Output Variables at Iteration i: $[\underline{\widehat{q}}^{(m)}]^{[i]}$, $[\underline{\widehat{r}_s}^{(m)}]^{[i]}$.

Given the input parameters, the EM algorithm for the i^{th} iteration is stated below.

Expectation Step (E-Step):

Calculate

$$\widehat{\widetilde{Q}}^{(m)} = \text{diag}\left\{[\underline{\widehat{q}}^{(m)}]^{[i-1]}\right\}, \tag{2.42}$$

where diag{ } converts the vector inside the associated braces into a diagonal matrix containing the vector's entries as the diagonal elements in the same order. Compute

$$\widetilde{Q} = \sum_{m=1}^{M} \widehat{\widetilde{Q}}^{(m)} \tag{2.43}$$

and

$$\alpha = \frac{\left[\text{trace}\left(\widehat{\widetilde{Q}}^{(m)}\right)\right]^2}{\left[\text{trace}\left(\widehat{\widetilde{Q}}\right)\right]^2}. \tag{2.44}$$

Calculate

$$\varrho_p^{(m)} = F_s \frac{\left\| [\underline{\widehat{r}_s}^{(m)}]^{[i-1]} - \underline{r_p} \right\|}{v}. \tag{2.45}$$

According to Eqs. (2.45), (2.6), (2.5), (2.4) and $a_p^{(m)} = 1, \forall p$ based on [53], determine $\underline{d}^{(m)}(k)$ and $\widetilde{D}(k)$. Next, follow Eqs. (2.19), (2.20), (2.26) to determine $\underline{\widehat{S}}(k)$ and $\widehat{S}^{(m)}(k)$, $k = 0, 1, \ldots, \jmath/2 - 1$, where $\widehat{S}^{(m)}(k)$ is the m^{th} element of $\underline{\widehat{S}}(k)$. Then determine

$$\underline{\widehat{X}}^{(m)}(k) = \mathbb{E}\left\{\underline{\widehat{X}}^{(m)}(k) \,|\, \underline{X}(k)\right\} = \underline{d}^{(m)}(k)\widehat{S}^{(m)}(k) + \alpha(\underline{X}(k) - \widetilde{D}(k)\underline{\widehat{S}}(k)), \;\; k = 0, 1, \ldots, \jmath/2 - 1. \tag{2.46}$$

Maximization Step (M-Step):

Now let

$$\varrho_p^{(m)} = F_s \frac{\left\| \underline{r_s}^{(m)} - \underline{r_p} \right\|}{v}, \tag{2.47}$$

where $\underline{r_s}^{(m)}$ is the variable coordinate and it has to be estimated in this step. Then, follow Eqs. (2.47), (2.6), and (2.5) to facilitate $\underline{d}^{(m)}(k)$, $k = 0, 1, \ldots, \jmath/2 - 1$, which involves the

variable coordinate $\underline{r_s}^{(m)}$. Then according to $\underline{d}^{(m)}(k)$, construct the following parameters

$$\underline{\dot{d}}^{(m)}(k) = \left(\widehat{\widetilde{Q}}^{(m)}\right)^{(-1/2)} \underline{d}^{(m)}(k), \;\; k = 0, 1, \ldots, \jmath/2 - 1, \tag{2.48}$$

which also involves the variable coordinate $\underline{r_s}^{(m)}$. According to the result from Eq. (2.46), calculate

$$\underline{\widehat{\dot{X}}}^{(m)}(k) = \left(\widehat{\widetilde{Q}}^{(m)}\right)^{(-1/2)} \underline{\widehat{X}}^{(m)}(k), \;\; k = 0, 1, \ldots, \jmath/2 - 1. \tag{2.49}$$

Then, construct

$$\underline{\widehat{g}}^{(m)}(k) = \underline{\widehat{X}}^{(m)}(k) - \underline{d}^{(m)}(k)\, \underline{\dot{d}}^{(m)}(k)^{\dagger} \underline{\widehat{\dot{X}}}^{(m)}(k), \;\; k = 0, 1, \ldots, \jmath/2 - 1, \tag{2.50}$$

which involves the variable coordinate $\underline{r_s}^{(m)}$ as well. Denote the p^{th} element of $\underline{\widehat{g}}^{(m)}(k)$ as $\widehat{g}_p^{(m)}(k)$. Facilitate

$$\underline{\widehat{g}_p}^{(m)} = \left[\widehat{g}_p^{(m)}(0), \;\; \cdots, \widehat{g}_p^{(m)}(\jmath/2 - 1)\right]^T, \tag{2.51}$$

which involves the variable coordinate $\underline{r_s}^{(m)} \in \mathcal{R}^{2\times 1}$. Carry out

$$[\underline{\widehat{r_s}}^{(m)}]^{[i]} = \underset{\underline{r_s}^{(m)}}{\arg\min} \sum_{p=1}^{P} \log\left(\left\|\underline{\widehat{g}_p}^{(m)}\right\|^2\right). \tag{2.52}$$

Besides, calculate $\varrho_p^{(m)} = F_s \frac{\left\|[\underline{\widehat{r}_s}^{(m)}]^{[i]} - \underline{r_p}\right\|}{v}$. Let $a_p^{(m)} = 1, \forall p$. Enumerate the parameters given by Eqs. (2.46), (2.6), (2.5), (2.33), (2.49), (2.50), and (2.51) in this sequential order. Then calculate

$$[\widehat{q_p}^{(m)}]^{[i]} = \frac{2}{\jmath}\left\|\underline{\widehat{g}_p}^{(m)}\right\|^2, \;\; p = 1, 2, \ldots, P. \tag{2.53}$$

Thus, obtain

$$[\underline{\widehat{q}}^{(m)}]^{[i]} = \left[[\widehat{q_1}^{(m)}]^{[i]}, \;\; \cdots, [\widehat{q_P}^{(m)}]^{[i]}\right]^T \in \mathcal{R}^{P\times 1}. \tag{2.54}$$

□

The above algorithm facilitates a recursive solution to multiple wide-band source localization. Note that the source location estimates $\underline{r_s}^{(m)}$, $m = 1, .., M$, can be carried out simultaneously in each iteration. Thus, the computational complexity can be greatly reduced if the parallel computation is feasible.

we provide the simulation results for our proposed EM source localization scheme in Section 2.1.3 and SC-ML method and AC-ML method in paper [53]. The sampling frequency is 100 kHz. The propagation speed is 345 meters/sec. The data is simulated for a circularly-shaped array of five sensors using the recorded acoustic data acquired from [53] as shown in Figure 2.2 (squares denote the sensor locations and circles denote the actual source locations). The sample size is $L = 200$ and the DFT size is $\jmath = 256$. Throughout the simulation, the minimization in our EM method characterized by Eq. (2.52) is performed by Nelder-Mead direct search [49], while the optimization steps in both SC-ML and AC-ML methods are performed using the alternating maximization (AM) algorithm, which would lead to better performance than Nelder-Mead direct search in these two schemes [49, 53]. Moreover, the additive noises in all experiments are randomly generated by a Gaussian process using the computer and the signal-to-noise ratio (SNR) is defined according to [53], [54].

Then we investigate the performance of the EM algorithm for estimating the two source locations in the presence of sensor noises with non-uniform variances, and compare with the SC-ML and AC-ML algorithms. The noise processes across different sensors have the covariance matrix as $\widetilde{Q} = \sigma^2 \, \mathrm{diag}\,\{2, 3, 1, 5, 9\}$. A hundred Monte Carlo experiments are carried out using our EM method with randomly initialized source locations for a particular signal-to-noise ratio (SNR=10 dB). The localization result from a certain experiment is depicted in Figure 2.2 where the ultimate locations are achieved after three iterations of EM

algorithm. We default the number of EM iterations as 3 in all Monte Carlo experiments. For each SNR value ranging from 0 to 40 dB, we fix the initial source location estimates as depicted in Figure 2.2 and carry out a hundred Monte Carlo experiments to obtain the average localization accuracy in terms of the root-mean-square (RMS) error in meters. The three corresponding RMS error curves to the three aforementioned schemes are depicted in Figure 2.3. Then, we vary the initial location estimates around the circular areas with a one-meter diameter with respect to the two initial source-location estimates depicted in Figure 2.2 and redo a hundred Monte Carlo experiments similar to the set-up generating Figure 2.3. The results are depicted in Figure 2.4. It is obvious that the accuracies of all three methods degrade from Figure 2.3 to Figure 2.4 since the initial conditions change. To further study this effect, we spread the initial location estimates over a broader area as depicted in Figure 2.5 and redo a hundred Monte Carlo experiments similar to Figure 2.4. The average RMS error curves are demonstrated in Figure 2.6.

Next, we would like to investigate the performances of the three aforementioned localization methods for the sensor noises with identical variances (SWN). Thus, we choose the sensor noise covariance matrix as $\widetilde{Q} = \sigma^2 \, \mathrm{diag}\{1, 1, 1, 1, 1\}$ now. With this new noise covariance matrix, we redo the Monte Carlo experiments similar to those generating Figures 2.3, 2.4, and 2.6. The corresponding results are plotted in Figures 2.7, 2.8, and 2.9, respectively. According to these two sets of experiments, our proposed EM algorithm greatly outperforms both SC-ML and AC-ML methods in all conditions. In addition, the accuracies of all three methods degrade due to the changes in the initial conditions for the SWN scenario as well. Besides, the performances of all these three schemes for the SWN case are not much different from those for the SNWN case, since the SWN model is a particular case of the SNWN model.

2.2 Computational Complexities Studies and Robustness Analysis for Source Localization Algorithms

In addition to the localization accuracy, the computational complexity is also an important factor to be considered in practice. Therefore, the studies of the computational complexities for three major source localization algorithms are presented in the following subsections.

2.2.1 Computational Complexities for Complex Multiplications

The first computational complexity comparison is focused on the required complex multiplications. For simplicity, in our computational complexity studies, we only consider the computational burden for the primary complex multiplications. The computations of the discrete Fourier transforms are neglected.

For our proposed EM method in Section 2.1.3, it requires $\frac{MP\jmath}{2}$ complex multiplications to carry out Eq. (2.46), where $\frac{MP\jmath}{2}$ and $M^2P\jmath$ multiplications respectively to determine $\widehat{\underline{S}}(k)$ and $\widetilde{D}(k)$ in Eq. (2.46), and $\frac{P\jmath}{2}$ multiplications to carry out Eq. (2.52), and $P\jmath + P^2\jmath$ multiplications to carry out Eq. (2.50) are also needed in addition. Consequently, in our proposed EM algorithm, the number of complex multiplications for M sources per iteration is

$$\kappa_{EM}^{\times} = M\left[\frac{\jmath}{2}P + P\jmath + P^2\jmath\right] + M^2P\jmath + MP\jmath. \tag{2.55}$$

If the parallel computation per iteration is allowed (given M microprocessors), the computational complexity per computer per iteration can be further reduced to

$$\kappa_{EM}^{\times} = \frac{\jmath}{2}P + P\jmath + P^2\jmath + M^2P\jmath + MP\jmath. \tag{2.56}$$

Two other existing source localization algorithms in [53] are compared here, namely *SC-ML* and *AC-ML* methods. The details of these two methods can be referred to as [53]. It is

easy to derive the number of complex multiplications for the SC-ML method, $\kappa^{\times}_{SC-ML}$, with respect to M sources per iteration such that

$$\kappa^{\times}_{SC-ML} = M\left[\frac{J}{2}P + \frac{J}{2}(2M^2P + P^2M + P^2)\right]. \tag{2.57}$$

On the other hand, the number of complex multiplications $\kappa^{\times}_{AC-ML}$ for the AC-ML method, with respect to M sources per iteration, is given by

$$\kappa^{\times}_{AC-ML} = (M+1)\left[\frac{J}{2}P + \frac{J}{2}(2M^2P + P^2M + P^2)\right]. \tag{2.58}$$

Note that both SC-ML and AC-ML methods in [53] cannot be decoupled across different sources for every iteration, and hence the complexity measures given by Eqs. (2.57) and (2.58) will not change even with the help of the parallel computation. Furthermore, from the simulation, we know that the EM, SC-ML, and AC-ML methods will need almost the same number of iterations to achieve the best results. Thus obviously, the complexity measure for our proposed algorithm given by Eq. (2.55) is in $\mathcal{O}(M^2)$ which is less than those for two other methods given by Eqs. (2.57) and (2.58) (in $\mathcal{O}(M^3)$). According to Eqs. (2.55), (2.57), and (2.58), we depict the computational complexity measures in terms of the required primary multiplications versus the number of sources (M) in Figure 2.10. As shown in Figure 2.10, the complexity difference between our proposed EM method and the two other methods is huge as the number of sources is large.

2.2.2 Computational Complexities for Minimization

Furthermore, the search for the minimum objective-function values is needed by all the three aforementioned schemes. For simplicity, we arbitrarily denote Υ by the computational complexity for the direct search method to determine a functional minimum. Assume that all

of the methods require ς iterations to achieve the final source location estimates. Hence, our proposed EM algorithm will require $M\varsigma\Upsilon$ totally for M sources. The SC-ML and AC-ML methods both also require the complexity of $M\varsigma\Upsilon$ for the optimization of the corresponding objective function since both schemes rely on the AM (alternating minimization) method [53]. With the help of the parallel computation, the complexity of our proposed EM algorithm can be further reduced as $\varsigma\Upsilon$ for the minimization of the objective function per computer. Nevertheless, the SC-ML and AC-ML algorithms have to undertake the minimum search for each source location estimate sequentially instead (impossible to benefit from the parallel computation) [53]. Thus, the EM method requires only $\frac{1}{M}$ times as many as the complexity of the SC-ML and AC-ML algorithms for seeking the objective-function minimum if the parallel computation is available.

2.2.3 Robustness Analysis for Source Localization Algorithms

Since the CRLB is the minimum achievable variance for any unbiased estimator, it is often used to characterize the robustness of the estimation methods. In this section, we derive the CRLB of the location estimates for the source localization problem by extending the CRLB in [53] for the simple DOA estimation problem.

By extending the CRLB presented in [53] for the DOA estimation problem, we derive the CRLB for the source localization problem to benchmark our EM method and the SC-ML/AC-ML schemes as

$$\frac{1}{\text{CRLB}} = 2\Re\left\{\sum_{k=0}^{\jmath/2-1}\left\{\left[\widetilde{\dot{G}}(k)^H \widetilde{P}^{\perp}_{\widetilde{D}(k)}\widetilde{\dot{G}}(k)\right]\odot \widetilde{R_s}(k)^T\right\}\right\}, \tag{2.59}$$

where

$$\widetilde{\dot{G}}(k) \stackrel{\text{def}}{=} \widetilde{Q}^{-1/2}\widetilde{G}(k), \tag{2.60}$$

$$\widetilde{G}(k) \stackrel{\text{def}}{=} \left[\frac{\partial}{\partial \underline{r_s}^{(1)}}\underline{d}^{(1)}(k), ..., \frac{\partial}{\partial \underline{r_s}^{(M)}}\underline{d}^{(M)}(k)\right], \tag{2.61}$$

$$\widetilde{P}^{\perp}_{\widetilde{\dot{D}}(k)} \stackrel{\text{def}}{=} \widetilde{I} - \widetilde{\dot{D}}(k)\widetilde{\dot{D}}(k)^{\dagger}, \tag{2.62}$$

$$\widetilde{R_s}(k) \stackrel{\text{def}}{=} \underline{S}(k)\underline{S}(k)^{H}. \tag{2.63}$$

Note that $\widetilde{Q}$, $\underline{d}^{(m)}(k)$, $\widetilde{\dot{D}}(k)$, and $\underline{S}(k)$ are given by Eqs. (2.8), (2.5), (2.20), (2.4), (2.7). We can rewrite Eq. (2.61) as

$$\widetilde{G}(k) = \frac{\partial \widetilde{D}(k)}{\partial \underline{r_s}^{T}} = -jF_s k\frac{2\pi}{v\jmath} \times \widetilde{F} \tag{2.64}$$

where

$$\widetilde{F} \stackrel{\text{def}}{=} \begin{bmatrix} a_1^{(1)}e^{-\frac{j2\pi k\varrho_1^{(1)}}{\jmath}}\underline{\lambda_1}^{(1)} & a_1^{(2)}e^{-\frac{j2\pi k\varrho_1^{(2)}}{\jmath}}\underline{\lambda_1}^{(2)} & \dots & a_1^{(M)}e^{-\frac{j2\pi k\varrho_1^{(M)}}{\jmath}}\underline{\lambda_1}^{(M)} \\ a_2^{(1)}e^{-\frac{j2\pi k\varrho_2^{(1)}}{\jmath}}\underline{\lambda_2}^{(1)} & a_2^{(2)}e^{-\frac{j2\pi k\varrho_2^{(2)}}{\jmath}}\underline{\lambda_2}^{(2)} & \dots & a_2^{(M)}e^{-\frac{j2\pi k\varrho_2^{(M)}}{\jmath}}\underline{\lambda_2}^{(M)} \\ \vdots & \vdots & \cdots & \vdots \\ a_P^{(1)}e^{-\frac{j2\pi k\varrho_P^{(1)}}{\jmath}}\underline{\lambda_P}^{(1)} & a_P^{(2)}e^{-\frac{j2\pi k\varrho_P^{(2)}}{\jmath}}\underline{\lambda_P}^{(2)} & \dots & a_P^{(M)}e^{-\frac{j2\pi k\varrho_P^{(M)}}{\jmath}}\underline{\lambda_P}^{(M)} \end{bmatrix} \in \mathcal{C}^{P\times 2M}, \tag{2.65}$$

$$\underline{\lambda_p}^{(m)} \stackrel{\text{def}}{=} \left[\frac{\partial d_p^{(m)}}{\partial \chi_s^{(m)}}, \frac{\partial d_p^{(m)}}{\partial y_s^{(m)}}\right] = \frac{\underline{r_s}^{(m)^T} - \underline{r_p}^{T}}{\|\underline{r_s}^{(m)} - \underline{r_p}\|} \in \mathcal{R}^{1\times 2}, \tag{2.66}$$

$$\frac{\partial d_p^{(m)}}{\partial \chi_s^{(m)}} = \frac{\chi_s^{(m)} - \chi_p}{\sqrt{\left(\chi_s^{(m)} - \chi_p\right)^2 + \left(y_s^{(m)} - y_p\right)^2}}, \tag{2.67}$$

$$\frac{\partial d_p^{(m)}}{\partial y_s^{(m)}} = \frac{y_s^{(m)} - y_p}{\sqrt{\left(\chi_s^{(m)} - \chi_p\right)^2 + \left(y_s^{(m)} - y_p\right)^2}}. \tag{2.68}$$

Note that $\underline{r_s}^{(m)} \stackrel{\text{def}}{=} [\chi_s^{(m)}, y_s^{(m)}]^T$ and $\underline{r_p} \stackrel{\text{def}}{=} [\chi_p, y_p]^T$ are used in Eq. (2.66).

We fix the initial source location estimates as those generating Figure 2.2 and carry out a

hundred Monte Carlo experiments again. The corresponding CRLBs for our EM method, the SC-ML (or AC-ML) method are depicted in Figure 2.11. We also depict the average RMS error curves in the same figure. According to Figure 2.11, we discover that the RMS errors resulted from our EM algorithm are much closer to the CRLBs than the SC-ML and AC-ML methods. Note that all the three source localization schemes in comparison are quite sensitive to the initial condition. This still remains as a very challenging problem for the wide-band source localization. Note that our experimental results illustrated in this paper can be generalized for other conditions. It means that if we change the source locations and use all the three algorithms subject to the same initial conditions, the experimental results under every different condition specified in Sections 2.1.3-2.2.3 will be very similar to Figures 2.3-2.11.

2.2.4 Conclusion

In this chapter, we propose a novel EM-based multiple wide-band source localization scheme in the presence of non-uniform noise variances. For our EM w method and the conventional SC-ML and AC-ML methods, the performance is rather sensitive to the initial source location estimates. Our proposed EM algorithm can lead to an outstanding localization performance given a reasonably good initial condition. Moreover, our proposed EM algorithm can always outperform the conventional SC-ML and AC-ML methods when the initial source location estimates are randomly chosen. The Monte Carlo simulation results demonstrate the superiority of our proposed EM method. To provide the robustness analysis for the source localization algorithms, we present the CRLB associated with these three schemes. The CRLB analysis demonstrates that our proposed EM algorithm is much closer to the

achievable minimum variance than the two other methods in all signal-to-noise ratio conditions. In addition, according to our complexity analysis, the complexity measure for our proposed algorithm is of $\mathcal{O}(M^2)$ which is much less than those for the SC-ML and AC-ML methods (both with a complexity measure of $\mathcal{O}(M^3)$).

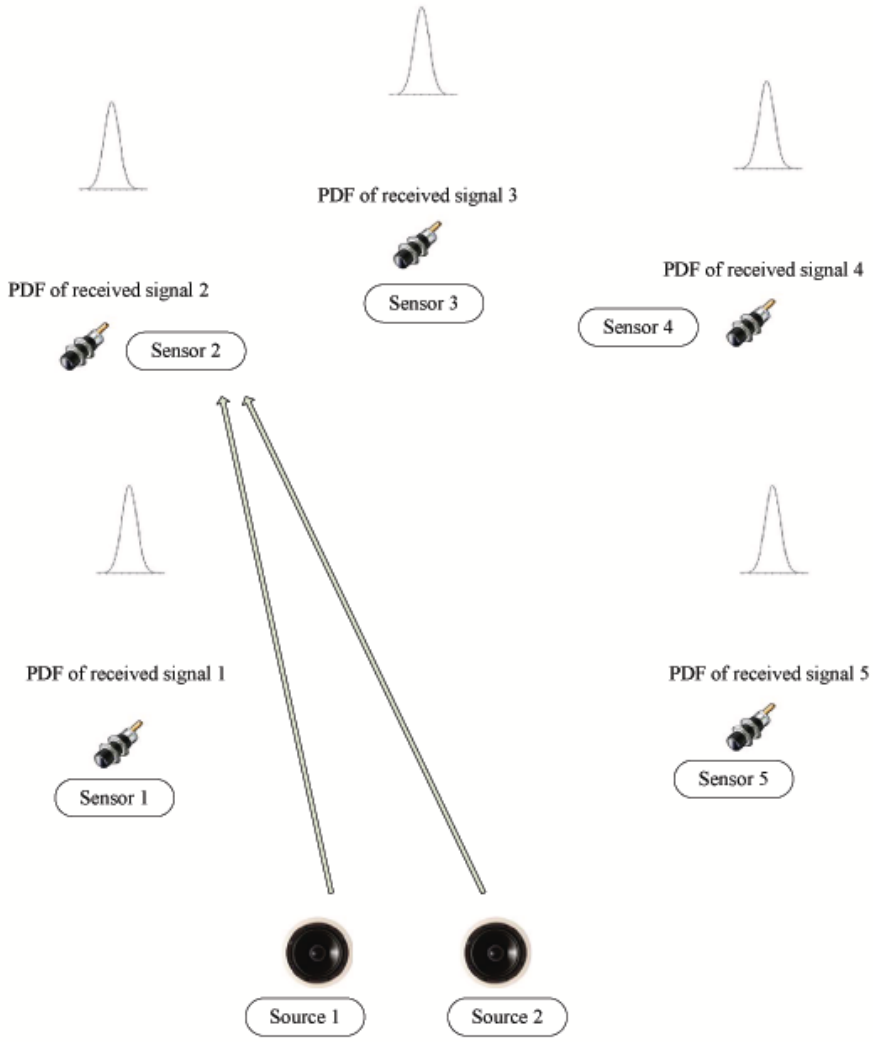

Figure 2.1: Localization of two wide-band sources in the near field.

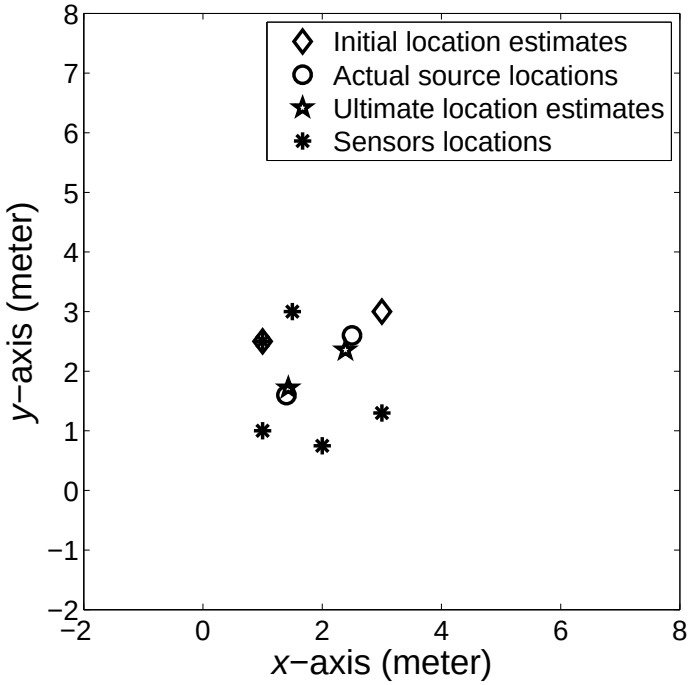

Figure 2.2: The localization of two wide-band (acoustic) sources in the near field corrupted by the noises with non-uniform variances (signal-to-noise ratio is 10 dB). The initial location estimates and the ultimate location estimates resulted from the EM algorithm (3 iterations are taken) are also demonstrated.

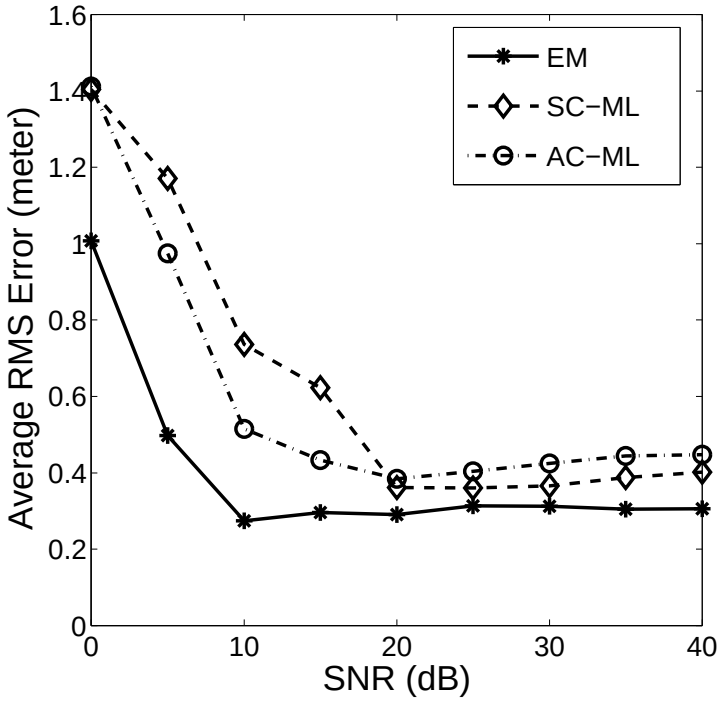

Figure 2.3: Average RMS localization errors versus SNR for the sources corrupted by the noises with non-uniform variances. The initial location estimates are plotted in Figure 2.2.

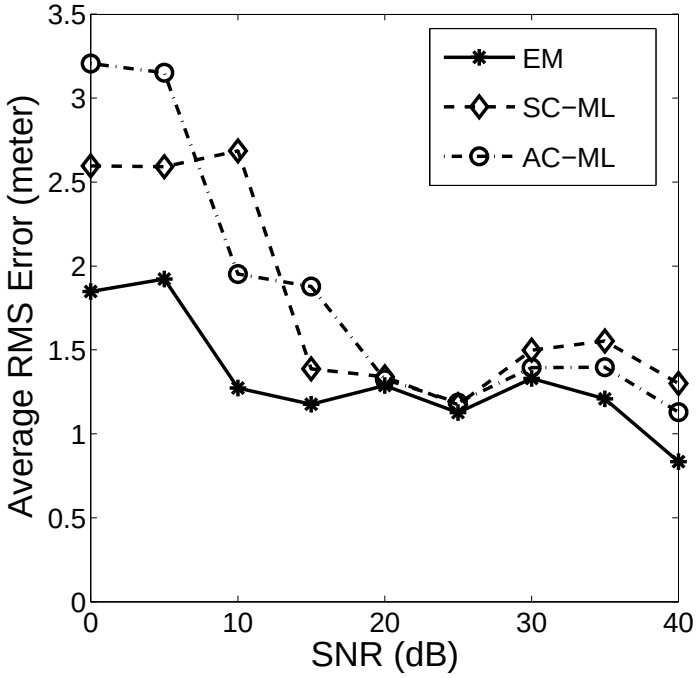

Figure 2.4: Average RMS localization errors versus SNR for the sources corrupted by the noises with non-uniform variances. The initial source location estimates here are randomly chosen within the areas which are one meter around the initial location estimates used in Figure 2.2.

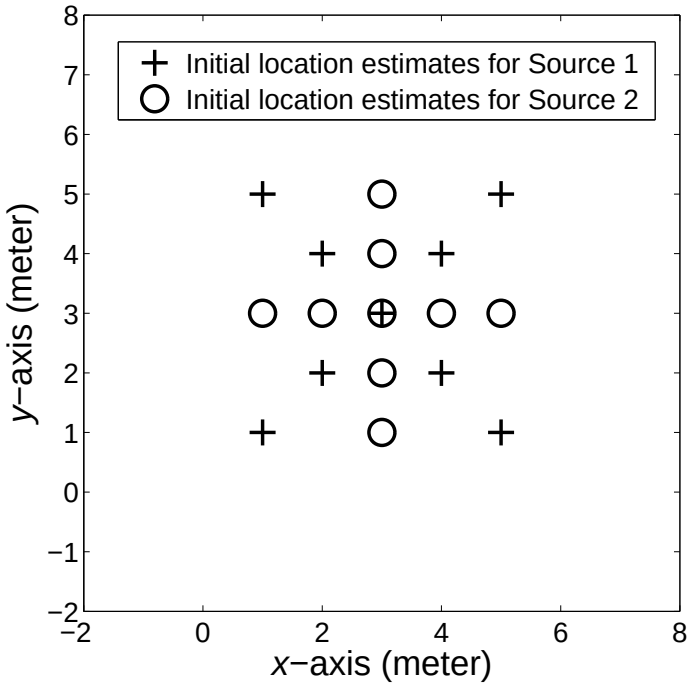

Figure 2.5: The eighteen different initial source location estimates.

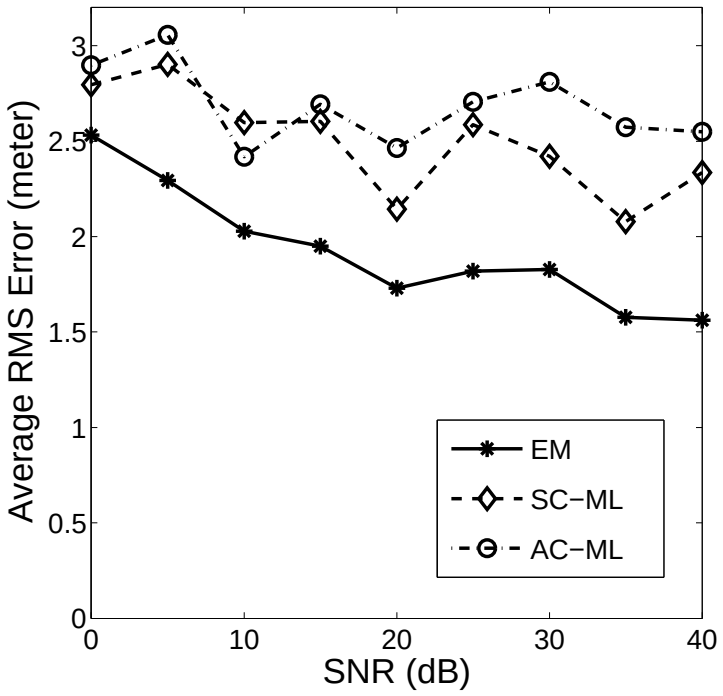

Figure 2.6: Average RMS localization errors versus SNR for the sources corrupted by the noises with non-uniform variances. The initial source location estimates are plotted in Figure 2.5.

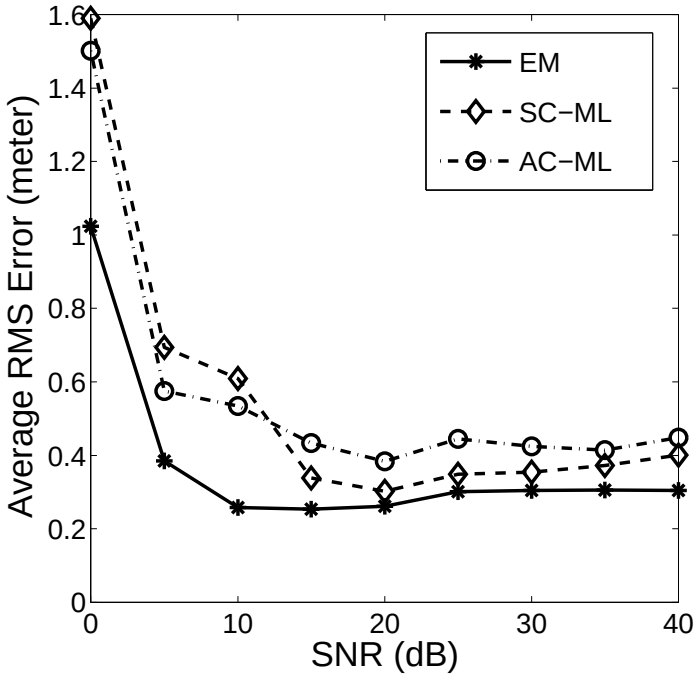

Figure 2.7: Average RMS localization errors versus SNR for the sources corrupted by the noises with identical variances. The initial source location estimates are plotted in Figure 2.2.

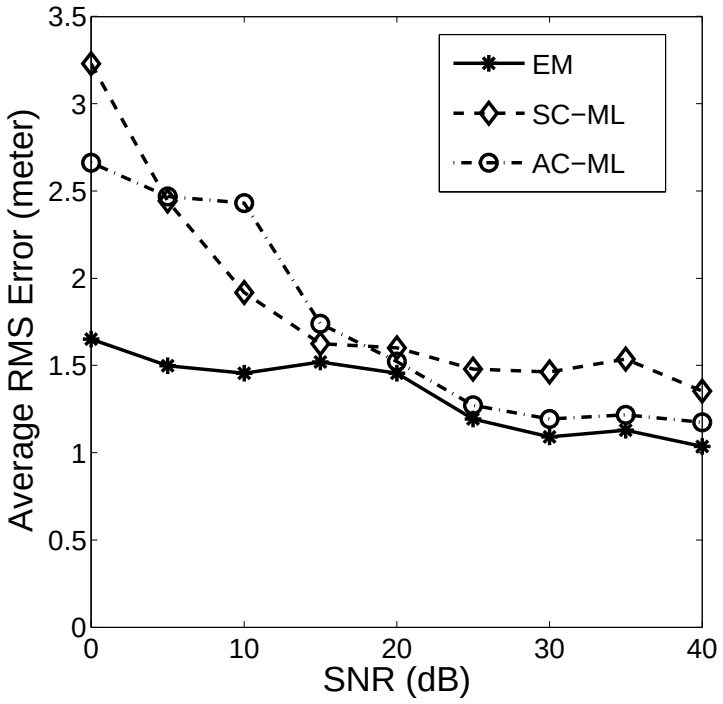

Figure 2.8: Average RMS localization errors versus SNR for the sources corrupted by the noises with identical variances. The initial source location estimates are randomly drawn from the areas which are one meter around the initial source location estimates in Figure 2.2.

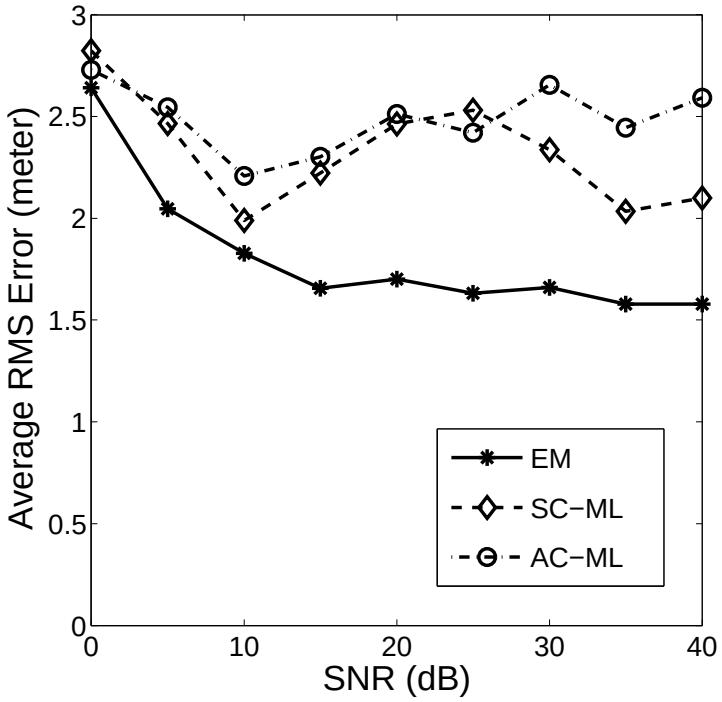

Figure 2.9: Average RMS localization errors versus SNR for the sources corrupted by the noises with identical variances. The initial source location estimates are plotted in Figure 2.5.

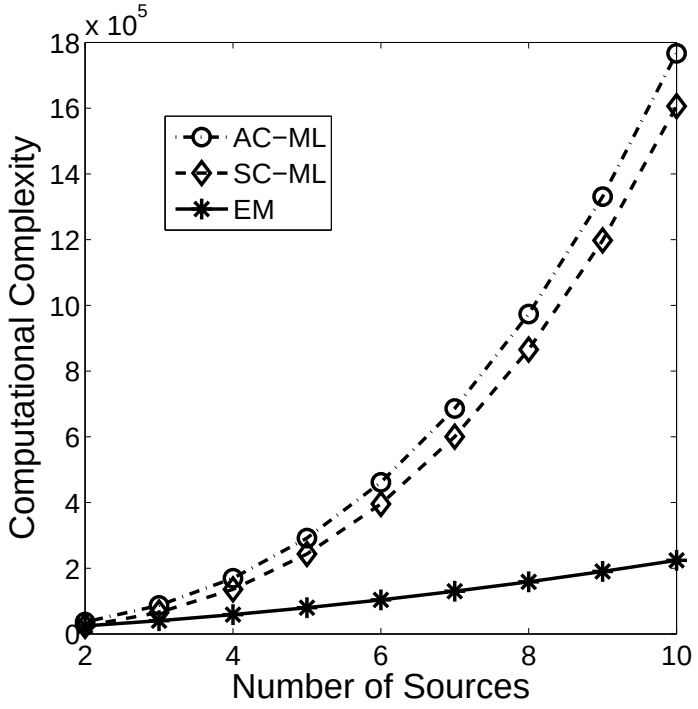

Figure 2.10: The computational complexity curves (the number of complex multiplications per iteration) versus the number of sources M for the three schemes in comparison ($J = 256$ and $P = 5$).

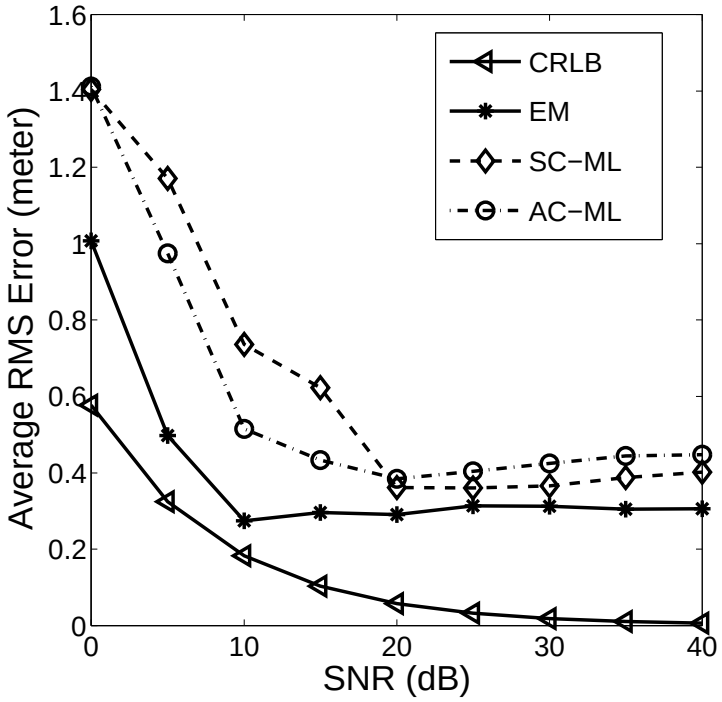

Figure 2.11: Cramer-Rao lower bounds and simulated (actual) RMS localization errors versus different SNR values for the three schemes in comparison.

3. NORMALITY TEST

In this chapter, we would like to tackle the normality test problem and it's applications for weak signal detection. Similar to the source localization problem in Chapter 2, normality tests can also be used for signal detection. The major difference between them is that normality tests can be carried out in the time domain and they can be based on a much simpler model than the source localization techniques. Besides, normality tests can be adopted for general signal detection purpose without any given knowledge about the source's spectral information such as frequency range which is required by source localization techniques.

3.1 Normality Test

The problem of identifying the probability distribution from which a particular random sample has been drawn is a naturally "fuzzy" problem: a given sample may, by chance, be drawn from any of an infinite number of quite different parent populations. Classification of random samples is a true example of uncertainty modeling. The greater part of modern statistical theory is built on the assumption that samples are drawn at random from underlying distributions which are normal. When sample size is large the issue of normality may be without practical significance because of the Central Limit Theorem, but when sample size is small the question of normality becomes important. Thus, in this chapter, we will propose a novel robust normality test which could be based on small sample size.

This chapter is organized as follows. In Section 3.1.2, we introduce the Kullback-Leibler divergence (KLD) studies to facilitate the Gaussianity analysis. In Section 3.1.3, the Gaussian and generalized Gaussian PDF models are employed to characterize the signal data's statistics under the Gaussian assumption. In Section 3.1.4, the skewness and the two-sample t-test are introduced to evaluate the symmetry of the actual PDF for the observations and they are very useful for further enhancing the robustness of the aforementioned KLD based Gaussianity test. In Sections 3.2.1 to 3.2.3, we present our novel Gaussianity test-KGGS test and its application for the weak signal detection [77, 78] of binary phase-shift keying (BPSK) and quadrature phase-shift keying (QPSK) signals. Conclusion will be drawn in Section 3.2.4.

3.1.1 Problem Definition

Let $f_{\mathbb{X}}(x)$ be an unknown distribution function of a real-valued stationary stochastic process $\mathbb{X}$ and suppose that we have $\mathbb{N}$ observations $x_1, x_2, \ldots, x_{\mathbb{N}}$ where each x_i is drawn from $\mathbb{X}$, $\forall i$. In general, we would like to check if $f_{\mathbb{X}}(x)$ can be considered Gaussian when the observations $x_1, x_2, \ldots, x_{\mathbb{N}}$ are given.

3.1.2 Kullback-Leibler Divergence Analysis

In the probability theory and the information theory, the Kullback-Leibler divergence is a non-commutative measure for quantifying the difference between two PDFs $f(x)$ and $q(x)$. Typically, $f(x)$ represents the true distribution of the random variable x or the *precisely calculated distribution*. The functional $q(x)$ denotes the approximation or the modeled PDF for $f(x)$. We assume that both functionals $f(x)$ and $q(x)$ satisfy the probability axioms and

the KLD between $f(x)$ and $q(x)$ is defined as

$$D_{\mathrm{KL}}(f \parallel q) \stackrel{\mathrm{def}}{=} \int_{-\infty}^{\infty} f(x) \log\left(\frac{f(x)}{q(x)}\right) dx. \tag{3.1}$$

Obviously, we have

$$\begin{aligned} D_{\mathrm{KL}}(f \parallel q) &= \int_{-\infty}^{\infty} f(x) \left(\log(f(x)) - log(q(x))\right) \\ &= \int_{-\infty}^{\infty} f(x) \log(f(x)) dx - \int_{-\infty}^{\infty} f(x) \log(q(x)) dx. \end{aligned} \tag{3.2}$$

In addition, as a result of Gibbs' inequality, the Kullback-Leibler divergence is always non-negative such that

$$\int_{-\infty}^{\infty} f(x) \log(f(x)) dx \geq \int_{-\infty}^{\infty} f(x) \log(q(x)) dx, \tag{3.3}$$

where the equality in (3.3) holds if any only if $f(x) = q(x)$. Note that the left-hand side of (3.3) depends only on the observations if $f(x)$ specifies the true PDF of the data while the right-hand side is subject to the chosen PDF model $q(x)$.

Let $\mathbb{N}$ real-valued independently identically distributed (i.i.d.) observations $x_1, x_2, \ldots, x_{\mathbb{N}}$ be drawn from a random process $\mathbb{X}$ and its true PDF is $f(x)$ but unknown. According to Eq. (3.2), the different choices for the PDF model $q(x)$ will only cause the variations in the second term $\int_{-\infty}^{\infty} f(x) \log(q(x)) dx$. Consequently, we can use this second term or its sample estimate as the sole measure to quantify how close $q(x)$ is to $f(x)$. It yields

$$\int_{-\infty}^{\infty} f(x) \log(q(x)) dx \approx \frac{1}{\mathbb{N}} \sum_{i=1}^{\mathbb{N}} \log(q(x_i)). \tag{3.4}$$

Eq. (3.4) manifests itself as a simple goodness-of-fit measure for a chosen PDF model $q(x)$ since it depends only on the PDF model functional $q(x)$ and the observed data $x_1, x_2, \ldots, x_{\mathbb{N}}$.

3.1.3 Gaussian and Generalized Gaussian PDFs

In order to establish the Gaussianity test using the KLD analysis stated in the previous section, we discuss two PDF models here.

Gaussian PDF Model

When the PDF model is chosen as Gaussian, we can write

$$q(x) = q_G(x) \stackrel{\text{def}}{=} \frac{1}{\sigma\sqrt{2\pi}} \exp\left(-\frac{(x-\mu)^2}{2\sigma^2}\right). \tag{3.5}$$

Since $x_1, ..., x_{\mathbb{N}}$ are i.i.d., the maximum likelihood estimates of the mean μ and the variance σ^2 are given by

$$\hat{\mu} = \frac{1}{\mathbb{N}} \sum_{i=1}^{\mathbb{N}} x_i, \tag{3.6}$$

$$\hat{\sigma^2} = \frac{1}{\mathbb{N}} \sum_{i=1}^{\mathbb{N}} (x_i - \hat{\mu})^2, \tag{3.7}$$

respectively. A Gaussian (normal) process is often expressed as $\mathbb{N}(\mu, \sigma)$.

Generalized Gaussian PDF Model

Next, we will also introduce the generalized Gaussian (GG) PDF model [79]. The PDF functional for the generalized Gaussian model is given by

$$q(x) = q_{\text{GG}}(x; \alpha, \beta) \stackrel{\text{def}}{=} \frac{\beta}{2\alpha\,\Gamma\left(\frac{1}{\beta}\right)} \exp\left\{-\frac{|x|^{\beta}}{\alpha}\right\}, \tag{3.8}$$

where α characterizes the width of the PDF peak (or standard deviation), β is inversely proportional to the functional decreasing rate from the peak value and $\Gamma(\ )$ denotes the Gamma function. Very often, α is referred to as the *scale parameter*, while β is called the *shape parameter*. The GG model constitutes many commonly-used PDF functionals such as

Gaussian ($\beta = 2$) and Laplacian ($\beta = 1$) distributions.

The maximum likelihood estimators for the parameters α and β can be found in [79]. We present them as follows. For the i.i.d. observations $x_1, x_2, \ldots, x_{\mathbb{N}}$, which belong to the random process $\mathbb{X}$, we can establish the log-likelihood function subject to the GG PDF as

$$L(\mathbb{X}; \alpha, \beta) = \log \left(\prod_{i=1}^{\mathbb{N}} q_{GG}(x_i; \alpha, \beta) \right), \tag{3.9}$$

where α and β are the parameters to be estimated. Maximizing $L(\mathbb{X}; \alpha, \beta)$, we get

$$\frac{\partial L(\mathbb{X}; \alpha, \beta)}{\partial \alpha} = -\frac{\mathbb{N}}{\alpha} + \sum_{i=1}^{\mathbb{N}} \frac{\beta \left| x_i \right|^{\beta} \alpha^{-\beta}}{\alpha} = 0. \tag{3.10}$$

Moreover,

$$\frac{\partial L(\mathbb{X}; \alpha, \beta)}{\partial \beta} = \frac{\mathbb{N}}{\beta} + \frac{\mathbb{N} \psi\left(\frac{1}{\beta}\right)}{\beta^2} - \sum_{i=1}^{\mathbb{N}} \left(\frac{|x_i|}{\alpha} \right)^{\beta} \log \left(\frac{|x_i|}{\alpha} \right) = 0, \tag{3.11}$$

where $\psi(\ )$ is the Digamma function ($\psi(z) \stackrel{\text{def}}{=} \left(\frac{d\Gamma(z)}{dz} \right) / \Gamma(z)$). Usually we fix $\beta > 0$. Then we obtain a unique, real, and positive solution to Eq. (3.10) as

$$\hat{\alpha} = \left(\frac{\beta}{\mathbb{N}} \sum_{i=1}^{\mathbb{N}} \left| x_i \right|^{\beta} \right)^{\frac{1}{\beta}}. \tag{3.12}$$

If we substitute Eq. (3.12) into Eq. (3.11), the solution of the following *transcendental equation* yields $\hat{\beta}$:

$$1 + \frac{\psi\left(\frac{1}{\hat{\beta}}\right)}{\hat{\beta}} - \frac{\sum_{i=1}^{\mathbb{N}} \left| x_i \right|^{\hat{\beta}} \log \left| x_i \right|}{\sum_{i=1}^{\mathbb{N}} \left| x_i \right|^{\hat{\beta}}} + \frac{\log \left(\frac{\hat{\beta}}{\mathbb{N}} \sum_{i=1}^{\mathbb{N}} \left| x_i \right|^{\hat{\beta}} \right)}{\hat{\beta}} = 0. \tag{3.13}$$

Although there exists no closed-form solution to Eq. (3.13), $\hat{\beta}$ can be solved numerically using the Newton-Raphson iterative procedure together with the initial guess from the moment method [79]. A generalized Gaussian process is often referred to as $GG(\alpha, \beta)$. The Gaussian and generalized Gaussian PDF functionals can effectively model $f(x)$ when it is actually

symmetric. However, when $f(x)$ is asymmetric, both PDF models cannot provide reliable estimates for the observations.

3.1.4 Skewness and Two-Sample t-Test

Skewness is a measure for the asymmetry of the probability distribution of any real-valued random variable. For $\mathbb{N}$ i.i.d. random samples $x_1, x_2, \ldots, x_{\mathbb{N}}$, its *sample skewness* $\hat{\varsigma}$ is given by

$$\hat{\varsigma} \stackrel{\text{def}}{=} \frac{\frac{1}{\mathbb{N}} \sum_{i=1}^{\mathbb{N}} (x_i - \hat{\mu})^3}{\left(\frac{1}{\mathbb{N}} \sum_{i=1}^{\mathbb{N}} (x_i - \hat{\mu})^2 \right)^{\frac{3}{2}}}, \tag{3.14}$$

where $\hat{\mu}$ is defined by Eq. (3.6). In addition, the skewness statistic can be transformed to satisfy the χ_1^2 distribution as follows:

$$\left(\frac{\hat{\varsigma}}{\sqrt{\frac{6}{\mathbb{N}}}} \right)^2 \sim \chi_1^2. \tag{3.15}$$

Thus, we can test the sample skewness according to Eqs. (3.14) and (3.15) for the PDF asymmetry.

The two-sample t-test is often used to determine if two population means are identical (for example, populations $\mathbb{X}_1$ and $\mathbb{X}_2$). When the sample size for both populations is equal to $\mathbb{N}$, the t-statistic to test whether their means are different or not is calculated as

$$t \stackrel{\text{def}}{=} \frac{\overline{\mathbb{X}}_1 - \overline{\mathbb{X}}_2}{S_{\mathbb{X}_1\mathbb{X}_2} \sqrt{\frac{2}{\mathbb{N}}}}, \tag{3.16}$$

where $S_{\mathbb{X}_1\mathbb{X}_2} \stackrel{\text{def}}{=} \sqrt{\frac{S_{\mathbb{X}_1}^2 + S_{\mathbb{X}_2}^2}{2}}$ ($S_{\mathbb{X}_1}$, $S_{\mathbb{X}_2}$ are the standard deviations for these two populations) and $\overline{\mathbb{X}}_1$, $\overline{\mathbb{X}}_2$ are the sample means for populations $\mathbb{X}_1$ and $\mathbb{X}_2$, respectively. For the significance test, t satisfies the t-distribution and the degree of freedom for this test is $2\mathbb{N} - 2$.

The t-test has a requirement that both populations should arise from the Gaussian distributions when the sample size is $\mathbb{N} \leq 30$. When the sample size gets larger ($\mathbb{N} \geq 100$), such a requirement is not necessary due to the central limit theorem.

3.2 New KGGS Test and Its Application for Signal Detection

According to our previous discussions in Sections 3.1.2-3.1.4, we design a new Gaussianity test, which in brief we call *Kullback-Leibler-Divergence Gaussian Generalized-Gaussian Skewness* (KGGS) test, as follows.

3.2.1 KGGS Test

Suppose that the observations $x_1, ..., x_{\mathbb{N}}$ are drawn from a stationary random process $\mathbb{X}$ whose true PDF $f(x)$ is unknown. We wish to check if these observation data fit the normal (Gaussian) distribution. From Section 3.1.2, we can use the sample average of $\log(q(x_i))$ to determine how well the model PDF $q(x)$ fits the underlying random process. In addition, according to our studies in Section 3.1.3, the Gaussian PDF model is a special case of the generalized Gaussian model with $\beta = 2$. It means that if we use both Gaussian and generalized Gaussian PDF models ($q_1(x)$ and $q_2(x)$ respectively) to fit the observations with the true normal distribution, then theoretically speaking, we get $f(x) = q_1(x) = q_2(x)$ and thus $\int_{-\infty}^{\infty} f(x) \log(q_1(x))\, dx = \int_{-\infty}^{\infty} f(x) \log(q_2(x))\, dx$. As the sample size approaches to infinity ($\mathbb{N} \to \infty$), there will appear to be very little difference in the sample averages of $\log(q_1(x_i))$ and $\log(q_2(x_i))$. However, for a random process $\mathbb{X}$ whose actual PDF $f(x)$ is not Gaussian and such difference would not be negligible. Hence we can establish a new

rule based on this difference in the two sample means of the two populations $\log(q_1(x_i))$ and $\log(q_2(x_i))$ to determine if the true PDF $f(x)$ of the random process $\mathbb{X}$ is the normal distribution.

The steps for our proposed new Gaussianity test are stated as follows:

Step 1) Use the Gaussian PDF to fit the observations $x_1, x_2, \ldots, x_{\mathbb{N}}$, estimate the sample mean $\hat{\mu}$ and variance $\hat{\sigma^2}$, and obtain the values of $\log(q_1(x_i))$, for $i = 1, 2, \ldots, \mathbb{N}$ where $q_1(x) = 1/(\hat{\sigma}\sqrt{2\pi}) \exp\big(-(x-\hat{\mu})^2/(2\hat{\sigma^2})\big)$.

Step 2) Use generalized Gaussian PDF to fit the observations instead and calculate the values of $\log(q_2(x_i))$, for $i = 1, 2, \ldots, \mathbb{N}$ where $q_2(x) = q_{\mathrm{GG}}(x; \hat{\alpha}, \hat{\beta})$ defined by Eq. (3.8). Note that the parameters $\hat{\alpha}$, $\hat{\beta}$ are estimated using Eqs. (3.12), (3.13).

Step 3) Use the composite rule to determine whether $f(x)$ is Gaussian or not (see below).

3.2.2 Composite Rule for Step 3 in 3.2.1

We will clearly describe the judgement rule for Step 3 in 3.2.1 now. As previously discussed, we use the differences $\frac{1}{\mathbb{N}}\sum_{i=1}^{\mathbb{N}} \log(q_1(x_i)) - \frac{1}{\mathbb{N}}\sum_{i=1}^{\mathbb{N}} \log(q_2(x_i))$, for $i = 1, \ldots, \mathbb{N}$, to determine if $f(x)$ is Gaussian. The proposed statistic is denoted by Υ such that

$$\Upsilon = \left| \left[\frac{1}{\mathbb{N}} \sum_{i=1}^{\mathbb{N}} \log(q_1(x_i)) - \frac{1}{\mathbb{N}} \sum_{i=1}^{\mathbb{N}} \log(q_2(x_i)) \right] \right|. \tag{3.17}$$

Theoretically speaking, if the random process $\mathbb{X}$ satisfies the Gaussian PDF and the sample size is infinity large, Υ in Eq. (3.17) should be zero. However, $\Upsilon \neq 0$ when $\mathbb{N}$ is finite. Note that $\Upsilon \to 0$ for a Gaussian random process $\mathbb{X}$ as $\mathbb{N} \to \infty$. Heuristically speaking, for a Gaussian process, Υ decreases from around 0.01 as $\mathbb{N}$ increases from 1. The judgement rule for Step 3 in 3.2.1 is split into the three parts as follows. Any random process will

be considered Gaussian only if all of the three following sub-tests justify this process as Gaussian.

Composite Rule Part (i)

First, Gaussian PDF and generalized Gaussian PDF models are both symmetric. If we use these two models to fit the random data with an asymmetrical distribution, the parametric estimation for $q_1(x)$ and $q_2(x)$ would be very unreliable. Consequently, the variation of Υ would arise and it leads to the inaccurate Gaussianity test. If the random process $\mathbb{X}$ has a normal distribution, its skewness should always be close to 0. Therefore, the skewness test as stated in Section 3.1.4 can be employed to reject the asymmetrically distributed data. In our scheme, we set the significance level of the skewness test to be 0.015. In other words, if the observations satisfy the normal distribution, then P value should be larger than 0.015, or otherwise we reject the Gaussian assumption. Note that setting $P = 0.015$ is equivalent to setting the threshold for $|\hat{\varsigma}|$ to be around 0.5. This is a very loose criterion for the Gaussianity test. The precise theoretical skewness value of a Gaussian process is 0 [56].

Composite Rule Part (ii)

Second, according to Stein's lemma in [80], the Kullback-Leibler divergence is the exponential rate of the optimal classifier performance probabilities. If $\mathbb{X}$ is a random vector consisting of $\mathbb{N}$ statistically independently and identically distributed components. We try to model these $\mathbb{N}$ random processes by $q_\alpha(x)$ or $q_\beta(x)$. The optimal classifier in the sense of maximum-likelihood results in the classification error probabilities with the following asymptotic identity:

$$\lim_{\mathbb{N}\to\infty} \log\left(\frac{P_F}{\mathbb{N}}\right) = -D_{\mathrm{KL}}\left(q_\alpha(x) \parallel q_\beta(x)\right), \tag{3.18}$$

where P_F is the corresponding false alarm rate. Specifically, if $\mathbb{X}$ has a normal distribution, its underlying statistical model fits both $q_1(x)$ and $q_2(x)$. Thus, according to Eq. (3.19), we can approximate the *optimal threshold* for Υ as $-\log\left(\frac{P_F}{\mathbb{N}}\right)$. When $\mathbb{N} = 250$ and $P_F = 0.05$, the threshold for Υ can be obtained as

$$\log\left(\frac{P_F}{\mathbb{N}}\right) \approx 0.01. \tag{3.19}$$

On the other hand, according to our simulation results, we have also found that for any non-Gaussian random process whose skewness is between -0.5 and 0.5, Υ does not have the monotonically decreasing trend towards 0 as $\mathbb{N}$ increases and Υ is seldom less than 0.01 when $\mathbb{N} \geq 250$. However, the value of Υ for a Gaussian process is rarely larger than 0.01 when $\mathbb{N} \geq 250$. Note that the larger $\mathbb{N}$, the smaller Υ for Gaussian processes. In fact, according to both our theoretical analysis and simulation results, $\Upsilon \leq 0.01$ when $\mathbb{N} \geq 250$, if the random data are normally distributed. In addition, we can choose a threshold of Υ smaller than 0.01 for a larger $\mathbb{N}$ according to Eq. (3.19). Generally speaking, the threshold 0.01 could be appropriate for a wide range of $\mathbb{N}$.

Composite Rule Part (*iii*)

Third, for any random process whose distribution is similar to Gaussian (but non-Gaussian), the Υ value is close to that resulting from a Gaussian process no matter how large $\mathbb{N}$ is chosen. In order to differentiate this subtle statistical discrepancy, we simply transform the two populations into $10^{\log(q_1(x_i))}$ and $10^{\log(q_2(x_i))}$, for $i = 1, \ldots, \mathbb{N}$, and then use the t-test with

a certain significance level to determine if they have the same means. If so, we accept the Gaussian assumption, or otherwise we reject this assumption.

We compare our KGGS test with other commonly-used normality tests, such as Pearson's χ^2 test, Shapiro-Wilk test, D'Agostino test, Jarque-Bera test and Lilliefors test. We randomly generate data samples associated with different PDFs to take 10,000 Monte Carlo trials. In each trial, we select two sample sizes as $\mathbb{N} = 250$, $\mathbb{N} = 500$ to imitate the sparse data and set the significance level as 0.05 to compare the rejection percentages arising from the aforementioned normality tests. The results are shown in Tables 4.1 and 4.2. Note that in all the tables and figures, the distributions are N: Normal, GG: Generalized Gaussian, U: Uniform, t: t-distribution, L: Laplacian, S: Alpha-Stable, W: Weibull, LN: Log-Normal, χ^2_8: chi-squared distribution (with mean 8), β: β-distribution, B: Binomial, E: Exponential, Γ: Gamma; SW stands for Shapiro-Wilk test; χ^2 stands for Pearson's χ^2 test; Dag stands for D'Agostino test; JB stands for Jarque-Bera test; Lillie stands for Lilliefors test. According to Tables 4.1 and 4.2, our proposed KGGS test can almost always outperform other existing tests in terms of these two objectives.

3.2.3 Our Proposed KGGS Test for Signal Detection

In practice, we can deem the observations $x_1, x_2, \ldots, x_{\mathbb{N}}$ as the received random signal traveling through the additive white Gaussian noise (AWGN) channel such that

$$x_i = s_i + w_i, \;\; i = 1, 2, \ldots, \mathbb{N}, \tag{3.20}$$

where s_i is the i-th transmitted information symbol and w_i, $i = 1, 2, \ldots, \mathbb{N}$, constitute an i.i.d. Gaussian process. The binary hypothesis test can be performed using the Bayesian criterion.

Table 3.1: Rejection Percentages for the Gaussian Hypothesis (at a 0.05 level of significance)

	$\mathbb{N} = 250$					
	KGGS	SW	χ^2	Dag	JB	Lillie
$N(0,1)$	0.05	0.05	0.05	0.05	0.05	0.05
$GG(1,1.8)$	15.70	8.61	6.20	11.10	12.09	8.12
$GG(1,1.5)$	62.64	38.32	15.93	40.39	44.97	29.55
$\beta(4,4)$	51.07	18.12	12.69	0.01	13.55	13.00
t_5	91.92	87.48	42.76	88.92	90.94	65.38
t_8	68.00	60.50	17.00	62.00	63.00	32.00
$L(0,1)$	100.00	99.00	92.10	97.80	98.60	98.30
$U(0,1)$	100.00	100.00	98.97	99.75	100.00	98.85
χ^2_8	100.00	100.00	97.50	100	100.00	98.40
$W(1,3)$	15.20	10.40	8.40	6.90	7.80	9.10
$\Gamma(100,1)$	15.00	14.80	8.00	14.00	14.00	11.00
$\Gamma(8,1)$	96.00	96.00	72.00	93.00	95.00	83.00
$S_{1.6}(1,0,0)$	100.00	99.90	96.60	99.80	99.90	98.70
$E(1)$	100.00	100.00	100.00	100.00	100.00	100.00

Table 3.2: Rejection Percentages for the Gaussian Hypothesis (at a 0.05 level of significance)

	$\mathbb{N} = 500$					
	KGGS	SW	χ^2	Dag	JB	Lillie
$N(0,1)$	0.05	0.05	0.05	0.05	0.05	0.05
$GG(1,1.8)$	22.10	10.80	6.70	14.80	17.80	10.40
$GG(1,1.5)$	87.50	63.10	32.30	65.70	70.00	53.30
$\beta(4,4)$	87.00	57.40	20.80	25.40	66.20	24.50
t_5	99.50	98.40	77.20	98.50	99.30	91.50
t_8	89.00	79.00	24.00	82.00	86.20	45.80
$L(0,1)$	100.00	100.00	99.90	100.00	100.00	99.90
$U(0,1)$	100.00	100.00	100.00	100.00	100.00	100.00
χ^2_8	100.00	100.00	100.00	100.00	100.00	100.00
$W(1,3)$	35.00	34.90	13.60	25.10	33.30	19.40
$\Gamma(100,1)$	29.10	28.70	13.10	28.80	28.30	22.80
$\Gamma(8,1)$	100.00	100.00	95.80	100.00	100.00	98.70
$S_{1.6}(1,0,0)$	100.00	100.00	100.00	100.00	100.00	100.00
$E(1)$	100.00	100.00	100.00	100.00	100.00	100.00

When s_i, $i = 1, 2, \ldots, \mathbb{N}$ are all drawn from a communication constellation, the conventional Bayesian hypothesis test involves the computationally-inefficient *clustering-and-estimating* classifier which is not robust when the sample size $\mathbb{N}$ is not large and/or the signal-to-noise ratio (SNR), $\mathbb{E}\{|s_i|^2\}/\mathbb{E}\{|w_i|^2\}$, is not large. The Gaussianity test would therefore be a good alternative. Thus, we would like to perform the weak BPSK (QPSK) signal detection subject to the transmission model given by Eq. (3.20). For both BPSK and QPSK cases, the sample size of the received signal is selected as $\mathbb{N} = 500$ and the SNR is set at -1 dB when the signal exists. For a variety of thresholds (confidence levels), 10,000 Monte Carlo runs are undertaken to compare the detection probabilities and the false alarm probabilities resulting from different normality tests. The receiver operating characteristic (ROC) curves are depicted in Figure 3.1 and Figure 3.2. They clearly demonstrate that our proposed KGGS test greatly outperforms all others for weak BPSK signal detection and weak QPSK signal detection.

3.2.4 Conclusion

In this chapter, we propose a novel normality test-KGGS test. When the sample size $\mathbb{N}$ is larger than 250, our proposed KGGS test is very robust for the random processes with symmetric distributions compared to other existing tests. In addition, we can apply our newly designed normality test for the weak signal detection. The receiver operating characteristic curves indicate the superiority of our proposed KGGS test to other existing normality tests. The normality test is an important and fundamental technique for a wide variety of engineering and scientific applications. Our robust KGGS test relying on a quite small sample size can be easily employed for many real-time signal processing systems.

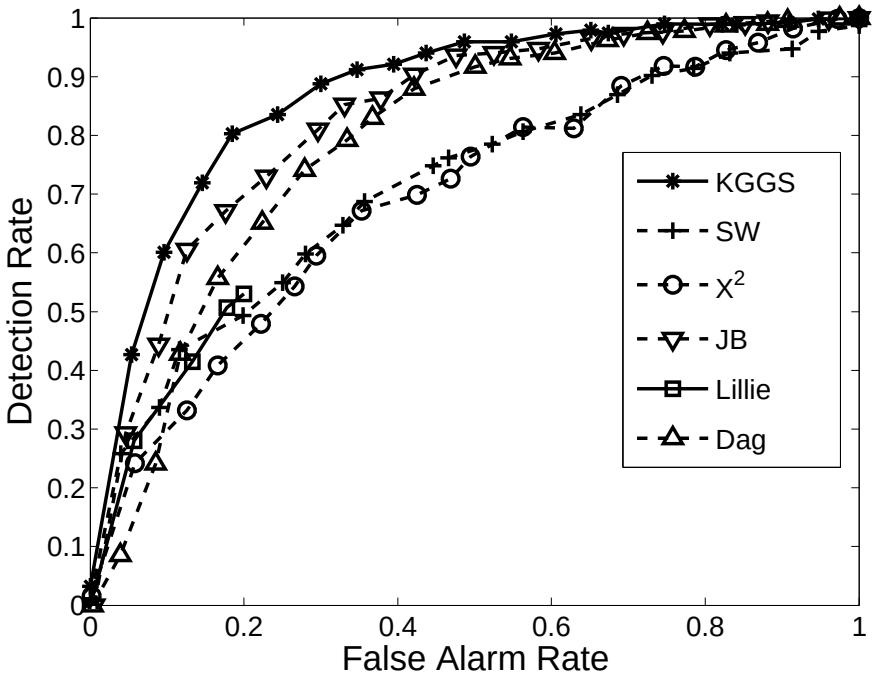

Figure 3.1: Receiver operating characteristic (ROC) curves for BPSK signal detection. Note that the confidence level for Lilliefors test can not exceed 0.2 (see [1]).

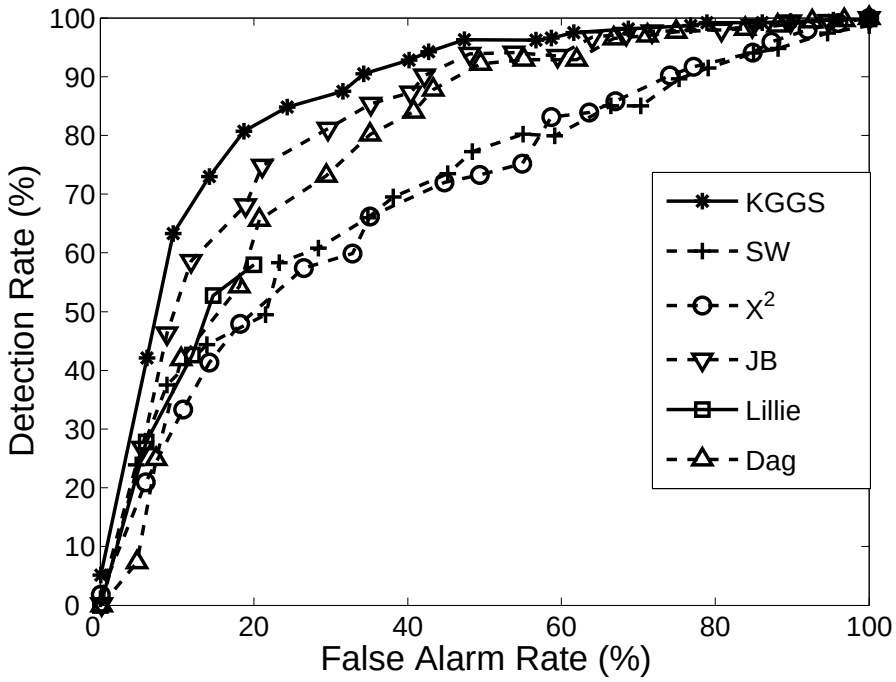

Figure 3.2: Receiver operating characteristic (ROC) curves for QPSK signal detection. Note that the confidence level for Lilliefors test can not exceed 0.2 (see [1]).

4. SPECTRUM SENSING[1]

In this chapter, we would like to investigate the spectrum sensing problem. Similar to source localization methods, spectrum sensing techniques would be quite sensitive to the sparsity and the weak signal conditions in practice. Therefore, the current challenges would be the demands for the robust and efficient methods (algorithms) for spectrum sensing. Spectrum sensing technology may be used to detect the existence of the operating wireless devices in the surrounding environment.

4.1 Spectrum Sensing

The topology of a wireless regional area network (WRAN) is illustrated in Fig. 4.1, where the primary users are television receivers, and the secondary users are WRAN base stations (BSs) and WRAN customer premise equipments (CPEs). The WRAN systems are designed to provide wireless broadband access to rural and suburban areas. The operating principle of WRAN is to provide any secondary user with an opportunistic access to the temporarily

[1] © [2011] IEEE. Reprinted, with permission, from [Lu Lu, Hsiao-Chun Wu and S.S. Iyengar, "A Novel Robust Detection Algorithm for Spectrum Sensing", IEEE Transactions on Selected Areas in Communications, February/2011].

unused TV spectrum. To avoid interference to the primary users, the secondary users can access to the TV channel only when the primary users are inactive. This concept is called *cognitive radio* [37].

This chapter is organized as follows. The problem formulation and the signal model are introduced in Section 4.1.1. The higher-order-statistics (HOS) based detection algorithm is introduced in Section 4.2.1. The novel Jarqur-Bera (JB) statistic based detection algorithm is derived and discussed in Section 4.2.2. Then the simulations for HOS detection and JB detection for DTV and microphone data are presented in Section 4.2.3. Next, the normality analysis for the received signal spectral waveform by Edgeworth Expansion method and KGGS test are presented in Sections 4.3.1 and 4.3.2. In addition, the spectral analysis for the received signal spectral waveform is stated in Section 4.3.3. The computational complexities analysis for HOS detection and JB detection are given in Section 4.3.4. Conclusion will be drawn in Section 4.3.5.

4.1.1 Problem Definition

Denote the continuous-time received signal by $r_c(t)$ during the sensing stage. The underlying signal from the primary users is denoted by $s_c(t)$ and $w_c(t)$ is the additive white Gaussian noise (AWGN). Hence, we have

$$r_c(t) \stackrel{\text{def}}{=} s_c(t) + w_c(t). \tag{4.1}$$

Assume that we are interested in the frequency band with the central frequency f_c and the bandwidth W. We sample the received signal at a sampling rate f_s, where $f_s \geq W$. Let $T_s = \frac{1}{f_s}$ be the sampling period and N be the sample size. For convenience, we denote

$$r_d(n) \stackrel{\text{def}}{=} r_c(nT_s), \;\; n = 1, \ldots, N, \tag{4.2}$$

$$s_d(n) \stackrel{\text{def}}{=} s_c(nT_s), \;\; n = 1, \ldots, N, \tag{4.3}$$

$$w_d(n) \stackrel{\text{def}}{=} w_c(nT_s), \;\; n = 1, \ldots, N. \tag{4.4}$$

According to [37], for the signal detection (spectrum sensing) problem, there involve two hypotheses, namely H_0: signal is absent and H_1: signal is present. The discrete-time received signals under these two hypotheses are given by

$$H_0 : r_d(n) = w_d(n), \tag{4.5}$$

$$H_1 : r_d(n) = s_d(n) + w_d(n), \tag{4.6}$$

where $r_d(n)$ denotes the received signal samples including the effect of path loss, multipath fading and time dispersion, and $w_d(n)$ is the discrete-time AWGN with zero mean and variance σ^2. Here $s_d(n)$ can be the superposition of the signals emitted from multiple primary users. When the received signal $r_d(n)$ consists of multiple sources (from either multiple independent sources or a single source signal traveling through multiple paths), it is usually modeled as the *correlated signal* [37]. It is assumed that signal and noise are uncorrelated with each other. The spectrum sensing (or signal detection) problem is therefore to determine whether the signal $s_d(n)$ exists or not, based on the received signal samples $r_d(n)$ [37, 72]. In reality, the recorded DTV channels are sampled at $f_s = 21.524476$ MHz and then down-converted to a low central intermediate frequency (IF) of 5.381119 MHz [81]. The acquired signal samples are used to detect if any DTV signal exists.

4.2 Efficient Spectrum Sensing Techniques

The signal detection has been a fundamental but ever-intriguing problem in telecommunications, signal processing, etc. The Bayesian hypothesis test has served as the mainstream theoretical framework for signal detection. However, the Bayesian classifier can be deemed optimal only when the complete statistic information is known for the observed signal. It is impossible in practice. Besides, the accurate probability density function (or the complete statistic information), which facilitates the Bayesian optimality, has to depend on a large amount of data and it is not feasible for low-cost, low-power, computationally-efficient handheld (mobile) devices. Instead of estimating the probability density function (PDF), the computationally-efficient detection methods using the partial statistics have been attracting a lot of research interest for decades. In this section, we first present an existing spectrum sensing technique based on the higher-order statistics. Then, we propose a novel spectrum sensing algorithm based on the JB-statistic, which is more robust than the former method especially when the sample size of the received signal is quite small.

4.2.1 Higher-Order-Statistics Spectrum-Sensing Algorithm

In this subsection, we will discuss about the higher-order-statistics (HOS) based detection algorithm (see [73]). This sensing technique is based on Gaussian noise statistics. The higher-order statistics can be used to evaluate how well the distribution of the test statistic matches a Gaussian distribution. In this method, the received signal is converted down to the baseband and then filtered. Next, the nominal ATSC pilot frequency is aligned to the DC and the down-converted signal is filtered again by a narrow-band low-pass filter. The resultant signal

is transformed to the frequency domain using the fast Fourier transform (FFT). Often, a 2,048-point FFT is recommended, since it is also used in the OFDM modulator/demodulator for the digital video broadcasting systems. Then, the higher-order moments and cumulants (higher than the second-order) for the real and imaginary parts of the signal spectra are calculated. If only noise is present, then the real and imaginary parts of the signal spectra are both Gaussian. The corresponding higher-order cumulants are thus all zero. Hence, in this sensing technique, a *Gaussianity test* is performed using the estimates of the higher-order cumulants. If it fails the Gaussianity test, then the hypothesis that the ATSC pilot signal is present holds true. The HOS detection algorithm has to use the third- to sixth-order cumulants and central moments [73]. The estimation variances of such high-order cumulants are usually quite large especially when the sample size is small [82]. Hence, it is obvious that the HOS approach cannot be robust when we do not have much received signal data or the channel model is time-varying. It motivates us to design a new spectrum sensing method to combat this problem.

4.2.2 Jarqur-Bera (JB) Statistic Based Detection Algorithm

Our goal is to design a robust spectrum sensing method involving estimates with less variances and leading to a computationally efficient solution. The JB statistic based on skewness and kurtosis is adopted here because kurtosis and skewness, which are composed by the second, third and fourth central moments only, could lead to more robust estimators than the HOS scheme relying on the higher-order moments or cumulants. Since JB statistic only depends on the second to fourth central moments, it would result in much less estimation variance than the variance of the HOS-based estimator (see [73, 82]) using the second to

sixth cumulants and central moments altogether according to the k-statistic and h-statistic theory. In addition, the HOS detection method (see [73]) tests the normality using the real and imaginary parts of the complex received samples subject to the property that all higher-order cumulants of a Gaussian PDF are zero. We propose to adopt the JB statistic to work on the norms of the complex signal samples, and the associated normality test is thus subject to the Rayleigh distribution instead. It is well known that the variance of a Gaussian process (for either its real or imaginary part) is much larger than the variance of the corresponding Rayleigh process (constituting the absolute values of the complex Gaussian random data). Hence, it can be foreseen that our proposed spectrum sensing method based on the signal norms can have the advantage over the method in [73]. Our proposed new spectrum sensing algorithm will be presented subsequently in Sections 4.2.2- 4.2.2.

Pre-Processing

The pre-processing steps in our proposed algorithm for transforming the received signal $r_d(n)$ into the frequency domain are the same as the HOS detection method [73]. Nevertheless, in our new detection method, we use the Jarque-Bera statistic of the signal spectrum's absolute values. The block diagram of our proposed new spectrum sensing method is depicted in Figure 4.2.

The signal flow in Figure 4.2 is described as follows. When the signal $r_d(n)$ is received, first we multiply $r_d(n)$ by $e^{-j2\pi f_c n T_s}$ to down-convert it to the baseband, where f_c is the low central IF frequency of 5.381119 MHz. Then, this baseband signal is sent through a digital image rejection low-pass (LP) filter with bandwidth $BW_r = 8 \times 10^6 \times \frac{2\pi}{f_s}$ radians. The image rejection filter is placed in the receiver so that the image frequencies along with

other unwanted signals are filtered out to enhance the signal quality.

Next, the enhanced signal $r_2(n)$ is further multiplied by $e^{-j2\pi f_v n T_s}$, where f_v=2.69 MHz. Then, the resulted signal $r_3(n)$ goes through the operations consisting of a down-sampler following a digital anti-aliasing filter whose bandwidth is given by

$$\mathrm{BW}_a = \frac{N_{\mathrm{FFT}}}{T_{\mathrm{sensing}}} \times \frac{2\pi}{f_s}, \tag{4.7}$$

where N_{FFT} is the FFT window size, and $T_{\mathrm{sensing}} = \frac{n}{f_s}$ is the sensing time. The down-sampling rate f_d is given by

$$f_d = \mathrm{floor}\left(\frac{2\pi}{BW_a}\right), \tag{4.8}$$

where the function "floor" is the operation to round $\frac{2\pi}{BW_a}$ to the nearest integer less than or equal to $\frac{2\pi}{BW_a}$. The down-sampled signal $r_5(n)$ is sent to a serial-to-parallel port and then the N_{FFT}-point FFT will be taken to result in a half-period FFT-sequence $R_{\mathrm{out}}(k)$, $k = 0, 1, \ldots, \frac{N_{\mathrm{FFT}}}{2} - 1$.

JB-Statistic Based Detection

In statistics, the Jarque-Bera test is a goodness-of-fit measure of departure from normality, based on the sample kurtosis and the sample skewness. The test is named after Carlos M. Jarque and Anil K. Bera. The test statistic, JB, is defined as

$$\mathrm{JB} \stackrel{\mathrm{def}}{=} \frac{n_s}{6}\left(\mathcal{S}^2 + \frac{(\mathcal{K}-3)^2}{4}\right), \tag{4.9}$$

where n_s is the number of observations (or degrees of freedom in general); $\mathcal{S}$ is the sample skewness and $\mathcal{K}$ is the sample kurtosis. They are defined as

$$\mathcal{S} \overset{\text{def}}{=} \frac{\hat{\mu}_3}{\hat{\sigma}^3} = \frac{\hat{\mu}_3}{(\hat{\sigma}^2)^{3/2}} = \frac{\frac{1}{n_s}\sum_{i=1}^{n_s}\left(\grave{x}_i - \bar{\grave{x}}\right)^3}{\left(\frac{1}{n_s}\sum_{i=1}^{n_s}\left(\grave{x}_i - \bar{\grave{x}}\right)^2\right)^{3/2}}, \tag{4.10}$$

$$\mathcal{K} \overset{\text{def}}{=} \frac{\hat{\mu}_4}{\hat{\sigma}^4} = \frac{\hat{\mu}_4}{(\hat{\sigma}^2)^2} = \frac{\frac{1}{n_s}\sum_{i=1}^{n_s}\left(\grave{x}_i - \bar{\grave{x}}\right)^4}{\left(\frac{1}{n_s}\sum_{i=1}^{n_s}\left(\grave{x}_i - \bar{\grave{x}}\right)^2\right)^2}, \tag{4.11}$$

where $\hat{\mu}_3$ and $\hat{\mu}_4$ are the estimates of the third and fourth central moments, respectively; $\grave{x}_i$, $i = 1, \ldots, n_s$ are the observations; $\bar{\grave{x}}$ is the sample mean and $\hat{\sigma}^2$ is the estimate of the second central moment or the variance. Therefore, this JB test can be considered as a sort of *portmanteau test*, since the four lowest moments about the origin are used jointly for its calculation.

Because $R_{\text{out}}(k)$, $k = 0, 1, \ldots, \frac{N_{\text{FFT}}}{2} - 1$ are complex-valued, if we try to directly apply JB test, we have to forsake either real-parts or imaginary-parts and thus the complete information is not utilized. For our proposed spectrum sensing method, we do not directly use the JB statistic as the conventional approach thereby. Here we check the absolute values of $R_{\text{out}}(k)$, $k = 0, 1, \ldots, \frac{N_{\text{FFT}}}{2} - 1$. Then, we invoke Eqs. (4.9), (4.10), and (4.11) to calculate the JB statistic of $|R_{\text{out}}(k)|$ and compare it with the threshold $r_{Threshold}$ to decide if there exists the signal $s_d(n)$. If JB $> r_{Threshold}$, we say that the signal exists; otherwise (JB $\leq r_{Threshold}$), we say that the signal is absent. We will present the theoretical study about how to select the threshold $r_{Threshold}$ subsequently.

Threshold Analysis for Our Proposed Method

In this subsection, we will discuss about how to select the threshold $r_{Threshold}$ for the proposed JB-statistic-based detection scheme according to both theoretical and heuristical analyses.

Let's review the Rayleigh distribution first, which is closely related to our proposed feature $|R_{\text{out}}(k)|$ under the JB test ($|R_{\text{out}}(k)|$ is Rayleigh distributed when signal is absent). The Rayleigh distribution is composed by random complex numbers whose real and imaginary components (x_{Real} and y_{Imag}) are both identically independently distributed (i.i.d.) Gaussian. The Rayleigh PDF with respect to $r = \sqrt{x^2 + y^2}$ is given by

$$f\left(r_{Rayleigh}; \sigma_r\right) = \frac{r_{Rayleigh}}{\sigma_r^2} \exp\left(\frac{-r_{Rayleigh}^2}{2\sigma_r^2}\right), \tag{4.12}$$

where $r_{Rayleigh} \in [0, +\infty)$, and σ_r is the mode. For the Rayleigh PDF given by Eq. (4.12), the skewness $\mathcal{S}_{\text{Rayleigh}}$ and the kurtosis $\mathcal{K}_{\text{Rayleigh}}$ are given as follows [83]:

$$\mathcal{S}_{\text{Rayleigh}} = \frac{2\sqrt{\pi}\,(\pi - 3)}{(4 - \pi)^{\frac{3}{2}}} \approx 0.631, \tag{4.13}$$

and

$$\mathcal{K}_{\text{Rayleigh}} = -\frac{6\pi^2 - 24\pi + 16}{(4 - \pi)^2} + 3 \approx -0.245 + 3 = 2.755. \tag{4.14}$$

When there is no signal, the input of the pre-processor (as presented in Section 4.2.2) is $r_d(n) = w_d(n)$. Then, after the pre-processing of the input signal, if there is no aliasing, the output $R_{\text{out}}(k)$, $k = 0, 1, \ldots, \frac{N_{\text{FFT}}}{2} - 1$ will be a complex Gaussian process whose real and imaginary components are both i.i.d. Gaussian. Thus, $|R_{\text{out}}(k)|$, $k = 0, 1, \ldots, \frac{N_{\text{FFT}}}{2} - 1$ will be Rayleigh-distributed. Substituting Eqs. (4.13) and (4.14) into Eq. (4.9), we can calculate the theoretical JB statistic value for Rayleigh distribution as $0.0344 N_{\text{FFT}}$ (here we set $n_s = \frac{N_{\text{FFT}}}{2}$). According to the central limit theorem and the law of large numbers, we know that when we apply different signal-absent observations ($r_d(n) = w_d(n)$) for $\hbar$ times ($\hbar$ is large enough), the JB statistic values in these different experiments will approximately satisfy a Gaussian distribution with a mean around $0.0344 N_{\text{FFT}}$. That is, the distribution of

these JB statistics will be approximately symmetric with respect to this mean. In addition, according to Eq. (4.9), the JB statistic is non-negative. It means that the smallest possible JB statistic value can only be zero, so subject to the symmetric property we can conclude that most (over 97% of the total population) of the JB statistic values will be smaller than twice of the mean $0.0344 N_{\mathrm{FFT}}$. On the other hand, if there is signal, $R_{\mathrm{out}}(k)$, $k = 0, 1, \ldots, \frac{N_{\mathrm{FFT}}}{2} - 1$ will not satisfy a Gaussian distribution. Thus, the skewness and the kurtosis of $|R_{\mathrm{out}}(k)|$, $k = 0, 1, \ldots, \frac{N_{\mathrm{FFT}}}{2} - 1$ would become larger. According to the aforementioned analysis, we set the threshold $r_{Threshold}$ for our JB-statistic based detector as

$$r_{Threshold} = 0.0688 N_{\mathrm{FFT}}. \tag{4.15}$$

For instance, when we select $N_{\mathrm{FFT}} = 2,048$, which is the defaulted FFT window size according to the DVB standards, the threshold will be $r_{Threshold} = 141$. Figure 4.3 depicts the histogram of the JB statistics for a complex Gaussian process over 1,000 random experiments. It can be clearly seen that all JB statistic values in Figure 4.3 are below the threshold $r_{Threshold} = 141$. In addition, the ensemble means of the calculated JB statistics and the (false-alarm) percentages of the JB statistics larger than $r_{Threshold} = 141$ are listed in Table 4.1. Provably, when the FFT window size is chosen as 2,048, the means of the JB statistics are always close to $0.0344 * 2048$. Its double, $r_{Threshold} = 141$, can be selected as the threshold, and the corresponding false alarms are always very small.

Table 4.1: JB Statistic Analysis

	Sample Size N					
	150,000	200,000	250,000	300,000	350,000	400,000
Mean	73.5	75.6	72.5	76.3	74.2	74.3
False-Alarm Percentage (JB > 141)	1%	2%	4%	3%	2%	3%

4.2.3 Simulation for HOS Detection and Our Proposed JB Detection

In our simulation, we test two types of commonly-used signals, namely DTV signal and microphone signal to benchmark the spectrum sensing methods. The simulation details are stated as follows.

Signal Acquisition and System Set-up

Subject to the IEEE 802.22 standard, the recorded DTV channels were sampled at 21.524476 Msamples/sec and then down-converted to a low central IF frequency of 5.381119 MHz (a fourth of the sampling rate). The real DTV data were acquired from [72]. On the other hand, according to [84], we simulate the microphone signal $s_{\text{mic}}(t)$ as follows:

$$s_{\text{mic}}(t) = \cos\left(2\pi \int_0^t \left[f_{cm} + f_{\triangle}\, w_m(\tau)\right] d\tau\right), \tag{4.16}$$

where f_{cm} is the same frequency as that of the DTV pilots; $f_{\triangle}$ is the frequency deviation around 100 KHz; $w_m(\tau)$ is the source signal which is randomly generated from the uniformly-distributed number in (-1,1). In addition, the sampling frequency for $s_{\text{mic}}(t)$ is 21.524476 MHz, which is the same as that of the captured DTV signal.

According to [85,86], the receiver noise characteristic consists of a typical noise power spectral density (PSD) and a noise uncertainty. The noise uncertainty specification is necessary since even though the sensing mechanism may involve calibration based on the noise power estimation, the estimate often exhibits some inaccuracy, which must be modeled. The thermal noise PSD is $N_0 = -174$ dBm/Hz. The receiver noise level is larger than the thermal noise level. Considering the effects of low-noise amplifier (LNA) noise figure, coupling losses, radio frequency (RF) switch losses and other issues, the TV industry typically specifies a *composite*

receiver noise figure of 11 dB. Hence the average receiver noise PSD is $\bar{N} = N_0 + 11 = -163$ dBm/Hz.

Moreover, according to the IEEE 802.22 document [81], for the purpose of employing the captured signal to evaluate different detection schemes, it is necessary to initially process the captured ATSC-DTV signals. In particular, the SNR can be precisely controlled in the same way by using this initial process for all different spectrum sensing methods. Quoted from [81], the specific steps for the initial process are given as follows.

Step 1): Read an appropriate number of samples from one of the DTV signal files.

Step 2): Filter the signal using a passband filter with a 6 MHz bandwidth and a center frequency of 5.38119 MHz. The filter shall be a "brick wall" filter (i.e. it shall have a flat frequency response with unity gain) which can allow some rare exceptions.

Step 3): Measure the power in the received signal.

Step 4): Generate white noise sampled at 21.524476 MHz and filter it through the same filter used in Step 2. The noise power used is the receiver noise power.

Step 5): Scale the signal power to meet the target SNR.

Step 6): Add the filtered noise with the scaled and filtered signal.

Spectrum Sensing Performance Comparison

In the following, we will present the simulation results for comparing our JB-statistic based detector and the HOS detector. First, the wireless microphone signals according to [72, 84] (randomly generated from computer) and the captured DTV signals from [72] (from the real world) are generated for the benchmark. In the simulation, we set $N_{\mathrm{FFT}} = 2048$, which is also used in the OFDM modulator/demodulator, N_{FFT} may vary. To the best of our

knowledge, the required sample size N is at least 100,000 for almost all existing spectrum sensing techniques [34, 37, 38, 72, 73]. However, our proposed JB detection method can easily rely on the relatively much smaller sample size around $N = 30,000$ to achieve satisfactory results.

In Figure 4.3, we set the sample size N as 150,000 and depict the histogram of the JB statistic values from 1000 random experiments. The associated means and the false-alarm rates (for the JB statistics which are larger than $r_{Threshold} = 141$) are listed in Table 4.1 for different N values. In Figure 4.4, we delineate the false detection rates resulting from the HOS detector and our JB-statistic based detector versus the sample size N in the sole presence of AWGN. According to Figure 4.4, it is obvious that when the sample size is larger than 50,000, both our JB-statistic based detector and the HOS detector have very low false detection rates. As the sample size gets smaller (< 50000), in other words, when the sensing time is short, the HOS detector leads to an extremely high false detection rate. Nevertheless, our proposed JB-statistic based detector can still work very well. In Figure 4.5, we depict the detection rates for the simulated wireless microphone signals from a single source over 1000 Monte Carlo experiments with $N = 70,000$ and $N = 150,000$, respectively. In Figure 4.6, we plot the detection rates for the real DTV signals from a single source over 1000 Monte Carlo experiments with $N = 70,000$ and $N = 150,000$, respectively. According to Figures 4.5 and 4.6, for the single-source case, our JB-statistic based detector always outperforms the HOS detector across different signal-to-noise ratios in terms of detection rate. Next, we will explore the multiple-source case, where the received signal is the correlated signal. In Figure 4.7, we plot the detection rates for the real DTV signals collected from two sources over 1000 Monte Carlo experiments with $N = 70,000$ and $N = 150,000$, respectively. In

this case, our JB-statistic based detector leads to a much better performance than the HOS detector, even when the sample size for the former method is 70,000 but that for the latter technique is 150,000. Obviously, the HOS detector does not work very well for the correlated signals.

4.3 Normality, Spectral and Computational Complexity Analysis

Via the thorough numerical evaluation, it is discovered that the performances of both our proposed JB detection method and HOS detection scheme significantly vary with respect to the sample size. The larger the sample size, the better the detection results. The HOS detection scheme is much more sensitive to the sample size. When the sample size is not sufficiently large (below 70,000), the HOS detection method would lead to a very high false alarm rate and fail. On the other hand, our proposed JB detection method can still lead to satisfactory results for the sample size is around 30,000. The reason is that when the sample size is small, $R_{\text{out}}(k)$, $k = 0, 1, \ldots, N_{\text{FFT}} - 1$ may not constitute a Gaussian process even in the sole presence of AWGN. To explain this interesting phenomenon, we first employ the Gaussianity test for the received signal involving the AWGN only.

The received signal spectral waveform as illustrated in Figure 4.2 is given by

$$\begin{aligned} R_{\text{out}}(k) &= \mathbf{Re}\left\{R_{\text{out}}(k)\right\} + \sqrt{-1}\ \mathbf{Im}\left\{R_{\text{out}}(k)\right\} \\ &= \sum_{n=0}^{N_{\text{FFT}}-1} \cos\left(\frac{2\pi kn}{N_{\text{FFT}}}\right) r_d(n) \qquad (4.17) \\ &\quad + \sqrt{-1} \sum_{n=0}^{N_{\text{FFT}}-1} \sin\left(\frac{2\pi kn}{N_{\text{FFT}}}\right) r_d(n), \\ &\quad k = 0, 1, \ldots, \frac{N_{\text{FFT}}}{2} - 1. \qquad (4.18) \end{aligned}$$

Note that for the HOS detection method, we have to use the full-period $R_{\text{out}}(k)$, $k = 0$, 1,

..., $N_{\mathrm{FFT}}-1$ instead. According to Eq. (4.17), we can measure the normalities separately for the real and imaginary parts of $R_{\mathrm{out}}(k)$. The following subsections are presented to study why $R_{\mathrm{out}}(k)$, $k=0,1,\ldots,N_{\mathrm{FFT}}-1$ do not satisfy the Gaussian assumption.

4.3.1 Edgeworth Expansion for PDF Characterization

As previously stated, the small sample size would often lead to the non-Gaussian characteristics of the received signals even in the sole presence of AWGN [87]. The Edgeworth expansion has been used to characterize the unknown PDF based on the estimated moments and cumulants. We adopt the Edgeworth expansion (see [88, 89]) to model the actual PDF of the aforementioned signal $\mathbf{Re}\{R_{\mathrm{out}}(k)\}$ and then evaluate the mismatch between the actual PDF and the underlying Gaussian model. Similar techniques can be used to study the statistical behavior for $\mathbf{Im}\{R_{\mathrm{out}}(k)\}$ as well and we omit this redundant discussion.

For a random variable Z ($Z=\mathbf{Re}\{R_{\mathrm{out}}(k)\}$ in our application here) with $E\{Z\}=0$ (this can always be achieved by creating a mean-removed variable $Z-E\{Z\}$) and unit variance, the arbitrary probability density function for Z can be written by Edgeworth expansion as:

$$f_Z(z)=\vartheta(z)\left\{1+\sum_{k=1}^{+\infty}P_k(z)\right\}, \tag{4.19}$$

where $\vartheta(z)$ is the zero-mean univariate Gaussian PDF, which is given by

$$\vartheta(z)\stackrel{\mathrm{def}}{=}\frac{1}{\sqrt{2\pi}}\exp\left(-\frac{z^2}{2}\right), \tag{4.20}$$

and $P_k(z)$ is a polynomial such that

$$P_k(z)\stackrel{\mathrm{def}}{=}\sum_{\{l_m\}}H_{k+2\varpi}(z)\prod_{m=1}^{k}\frac{1}{l_m!}\left(\frac{\chi_{m+2}}{(m+2)!}\right)^{l_m}. \tag{4.21}$$

Here the set $\{l_m\}$ consists of all non-negative integer solutions to the equation $l_1+2l_2+\ldots+kl_k=k$, and $\varpi=l_1+l_2+\ldots+l_k$, and χ_l is given by

$$\chi_l = (-1)^l \frac{d^l}{d\eta^l} \log \hat{f}_Z(\eta)\Big|_{\eta=0}, \tag{4.22}$$

where $\hat{f}_Z(\eta) \stackrel{\text{def}}{=} E\{e^{jz\eta}\}$ is the characteristic function of $\mathbf{Re}\{R_{\text{out}}(k)\}$ and $H_l(z)$ is the l^{th}-order Hermite polynomial such that

$$\vartheta(z)H_l(z) = (-1)^l \frac{d^l}{dz^l}\vartheta(z). \tag{4.23}$$

Later on, we will compare the actual PDF given by Eq. (4.19) with the Gaussian model given by Eq. (4.20) for $Z = \mathbf{Re}\{R_{\text{out}}(k)\}$ to test if there is significant statistical mismatch in between.

In Figures 4.8 and 4.9, we use the Edgeworth expansion and the Gaussian model to characterize the PDFs for the full-period signal sequence $Z = R_{\text{out}}(k)$, $k = 0, 1, \ldots, N_{\text{FFT}} - 1$ and the half-period signal sequence $Z = R_{\text{out}}(k)$, $k = 0, 1, \ldots, \frac{N_{\text{FFT}}}{2} - 1$ in the sole presence of AWGN ($r_d(n)$=$wd(n)$). The sample sizes in Figure 4.8 and Figure 4.9 are $N = 30000$ and $N = 70000$, respectively.

4.3.2 Gaussianity Measure Using KGGS Test

Although the Edgeworth expansion can help us to obtain the complete "actual PDF", it cannot provide a simple (scalar) measure for the aforementioned mismatch in practice. We propose to use the KGGS test stated in Chapter 3 for the robustness analysis of both our JB detection method and the HOS detection scheme. Note that in the KGGS test, for the JB detection method, the sample size is $\mathbb{M} = \frac{N_{\text{FFT}}}{2}$ while for the HOS detection method, the sample size is $\mathbb{M} = N_{\text{FFT}}$ instead. For the two sets of data in Figures 4.8 and 4.9, we perform the KGGS test to check the normality. The results of the KGGS test are given in Table 4.2.

According to Table 4.2, the rejection percentages are very high for the normality assumption when the sample size N is not large enough. It clearly shows that the raw feature of $R_{\text{out}}(k)$ used in the HOS detector is not robust when only a few dozens of thousands of samples are acquired or when the sensing time is short.

Table 4.2: Rejection Rates of KGGS Normality Test

	N						
	20,000	30,000	40,000	50,000	60,000	70,000	80,000
$\mathbb{M} = N_{\text{FFT}}$	100%	100%	100%	100%	100%	11%	0%
$\mathbb{M} = \frac{N_{\text{FFT}}}{2}$	76%	12%	8%	7%	7%	5%	0%

4.3.3 Spectral Analysis

As previously mentioned, our JB detection method depends on $|R_{\text{out}}(k)|$, $k = 0, 1, \ldots, \frac{N_{\text{FFT}}}{2} - 1$, but the HOS detection method depends on $R_{\text{out}}(k)$, $k = 0, 1, \ldots, N_{\text{FFT}} - 1$ instead. In this subsection, we will explain the reason why our method does not rely on $R_{\text{out}}(k)$, $k = 0, 1, \ldots, N_{\text{FFT}} - 1$ as the HOS detection method. The frequency spectrum of the sampled received DTV signal $r_d(n)$ has a bandwidth of $6 \times 10^6 \times \frac{2\pi}{f_s}$ radians and a central frequency $5.38119 \times 10^6 \times \frac{2\pi}{f_s}$ radians according to [81]. According to Figure 4.2, after down-conversion, image rejection and frequency shifting, the spectrum of the signal $r_3(n)$ will occupy the digital frequency intervals ranging from 0 to $5.69 \times 10^6 \times \frac{2\pi}{f_s} = 0.5288\pi$ radians (with a bandwidth 0.5288π radians) over $[0, \pi]$, and ranging from $2\pi - (6 - 5.69) \times 10^6 \times \frac{2\pi}{f_s} = 1.9712\pi$ to 2π radians (with a bandwidth 0.0288π) over $[\pi, 2\pi)$. Due to the frequency-shifting operations in Figure 4.2, it can be seen that the magnitude spectrum of $r_3(n)$ is definitely not symmetric over $[-\pi, \pi]$. Next, let the signal $r_3(n)$ pass the low-pass filter with a bandwidth BW_a specified by Eq. (4.7), and down-sample $r_4(n)$ with a down-sampling

rate f_d given by Eq. (4.8). The half-period FFT sequence $R_{\text{out}}(k)$, $k = 0, 1, \ldots, \frac{N_{\text{FFT}}}{2} - 1$ should correspond to the digital frequency interval $[0, \pi]$ in where $|R_{\text{out}}(k)|$ would not have any null band. However, the signal spectrum $R_{\text{out}}(k)$, $k = \frac{N_{\text{FFT}}}{2}, \frac{N_{\text{FFT}}}{2} + 1, \ldots, N_{\text{FFT}} - 1$ corresponding to $[\pi, 2\pi)$ would exhibit a null band especially when the sample size N is smaller than the threshold number ν (ν will be defined in Eq. (4.24)) which makes the low-pass filter possess a bandwidth of 0.0288π radians (this bandwidth is identical to the signal bandwidth within $[\pi, 2\pi)$). In other words, we will have $R_{\text{out}}(k) = 0$, for some k values when the sample size N is smaller than ν. Besides, if the null band of $R_{\text{out}}(k)$ is too broad, $R_{\text{out}}(k)$, $k = 0, 1, \ldots, N_{\text{FFT}} - 1$ would not fit the complex Gaussian distribution even in the sole presence of AWGN. Thus when the sample size N is not large enough, if we use the full-period $R_{\text{out}}(k)$, $k = 0, 1, \ldots, N_{\text{FFT}} - 1$ for the spectrum sensing, it will lead to a very high false alarm rate and the result is not satisfactory. This is the very reason why the HOS detection method often leads to a very high false alarm rate when the sample size N is small. It is also the reason why our JB detection scheme should rely on the half-period $R_{\text{out}}(k)$, $k = 0, 1, \ldots, \frac{N_{\text{FFT}}}{2} - 1$. Based on the previous discussion, the theoretical value for ν can be calculated as

$$\nu = \frac{\pi}{0.0288\pi} \times N_{\text{FFT}}. \tag{4.24}$$

Eq. (4.24) facilitates the sample size N for the down-sampling rate $f_d = \frac{\pi}{0.0288\pi}$. In other words, the minimum sample size $N = \nu$ is required for the HOS detection method to work. For example, when the FFT window size is set as $N_{\text{FFT}} = 2048$, we need $N \geq \nu \approx 71,000$. The effects of sample size can also be found in our previous discussions in Sections 4.3.1, 4.3.2 and in the subsequent simulations.

According to Table 4.2, the rejection percentages are very high for the normality assumption when the sample size N is not large enough. It clearly shows that the raw feature of $R_{\text{out}}(k)$ used in the HOS detector is not robust when only a few dozens of thousands of samples are acquired or when the sensing time is short. To get more insights into this discovery, we provide Figures 4.10 and 4.11 to show the magnitude frequency spectra $|R_{\text{out}}(k)|$, $k = 0, 1, \ldots, N_{\text{FFT}}-1$ for $N = 30000$ and $N = 70000$, respectively. It can be easily seen that there exist *null bands* in the signal spectra as depicted by Figures 4.10 and 4.11 and such null bands would easily destroy the normality and degrade the detection performance. Besides, the bandwidth of such a null band increases as the sample size decreases. Hence, the full-period feature $R_{\text{out}}(k)$ adopted in the HOS detector may not lead to robust performance. According to Figures 4.8-4.11 and Table 4.2, we can justify our arguments stated in Section 4.3. When the sample size N is not sufficiently large, the underlying full-period feature $R_{\text{out}}(k)$, $k = 0, 1, \ldots, N_{\text{FFT}} - 1$ used in the HOS detector does not satisfy the Gaussian assumption, but the half-period feature $R_{\text{out}}(k)$, $k = 0, 1, \ldots, \frac{N_{\text{FFT}}}{2} - 1$ would much better fit the Gaussian hypothesis. Next we would like to investigate how the HOS detector performs if it also uses the half-period feature $R_{\text{out}}(k)$, $k = 0, 1, \ldots, \frac{N_{\text{FFT}}}{2} - 1$. In Figure 4.12, we use the half-period feature $R_{\text{out}}(k)$ instead in the HOS detector and depict the corresponding detection rates. The detection rates are similar to those arising from the aforementioned HOS detector and still lower than the results from our proposed JB statistic based detector.

4.3.4 Computational Complexity Analysis

The computational complexity is always an important factor to be considered in practice. Therefore, the computational complexity studies for our JB detection method and

HOS detection method are presented in this section. For simplicity, here we only consider the real-valued multiplications in studying the complexity. Thus, the computational complexity analysis for the two aforementioned detectors is presented as follows. For our proposed JB statistic-based detector, we need to take $4 \times \frac{N_{\mathrm{FFT}}}{2}$ multiplications to calculate the absolute values of $R_{\mathrm{out}}(k),\ 0, 1, \ldots, \frac{N_{\mathrm{FFT}}}{2} - 1$. Moreover, in order to obtain $\mathcal{S}$ and $\mathcal{K}$ in Eqs. (4.10) and (4.11), we need to compute the second, third, and fourth moments of $|R_{\mathrm{out}}(k)|,\ 0, 1, \ldots, \frac{N_{\mathrm{FFT}}}{2} - 1$. Hence, we need to take $3 \times \frac{N_{\mathrm{FFT}}}{2}$ multiplications for achieving that. At last, we need one more comparison operation to carry out the ultimate hypothesis test. In total, for our JB statistic-based detection, the complexity $\mathbb{C}_{\mathrm{JB}}$ (in terms of multiplications) is given by

$$\mathbb{C}_{\mathrm{JB}} = 7 \times \frac{N_{\mathrm{FFT}}}{2} + 1 = 3.5\, N_{\mathrm{FFT}} + 1. \tag{4.25}$$

The HOS detection method in [73] depends on $R_{\mathrm{out}}(k),\ k = 0, 1, \ldots, N_{\mathrm{FFT}} - 1$. It needs to take $10 \times N_{\mathrm{FFT}}$ multiplications to calculate the second to sixth moments of both real and imaginary parts of $R_{\mathrm{out}}(k)$. Furthermore, it needs 10 multiplications to calculate the required cumulants, and needs to take 3 comparison operations for the ultimate hypothesis test. Therefore, its total computational complexity $\mathbb{C}_{\mathrm{HOS}}$ is

$$\mathbb{C}_{\mathrm{HOS}} = 10 \times N_{\mathrm{FFT}} + 13. \tag{4.26}$$

Usually, we choose N_{FFT} to be 2,048, so it is obvious that our proposed JB-statistic based detector is much more computationally efficient than the HOS detector. We also depict the trends of the computational complexities versus different N_{FFT} for these two detectors in the next section. To compare the complexity measures in numerical illustration, Figure 4.13

depicts the computational complexities in terms of multiplications for the HOS detection method and our proposed detector. It clearly shows that our method is much more efficient.

4.3.5 Conclusion

In this chapter, we propose a novel JB-statistic based spectrum sensing method, which can be applied for the IEEE 802.22 systems. Our method outperforms the existing HOS detection scheme which is based on the higher-order statistics. According to our Monte Carlo simulation results for the simulated wireless microphone signals and the real DTV signals, our proposed JB detection method not only leads to a higher detection rate but also induces less computational complexity than the HOS detector. Besides, our proposed JB-statistic based detector can be very robust for the small sample size or the short sensing time. We also provide the normality analysis and the spectral analysis to explore the reasons why our proposed detector has the significant advantages over the HOS detection method especially when the sample size is small.

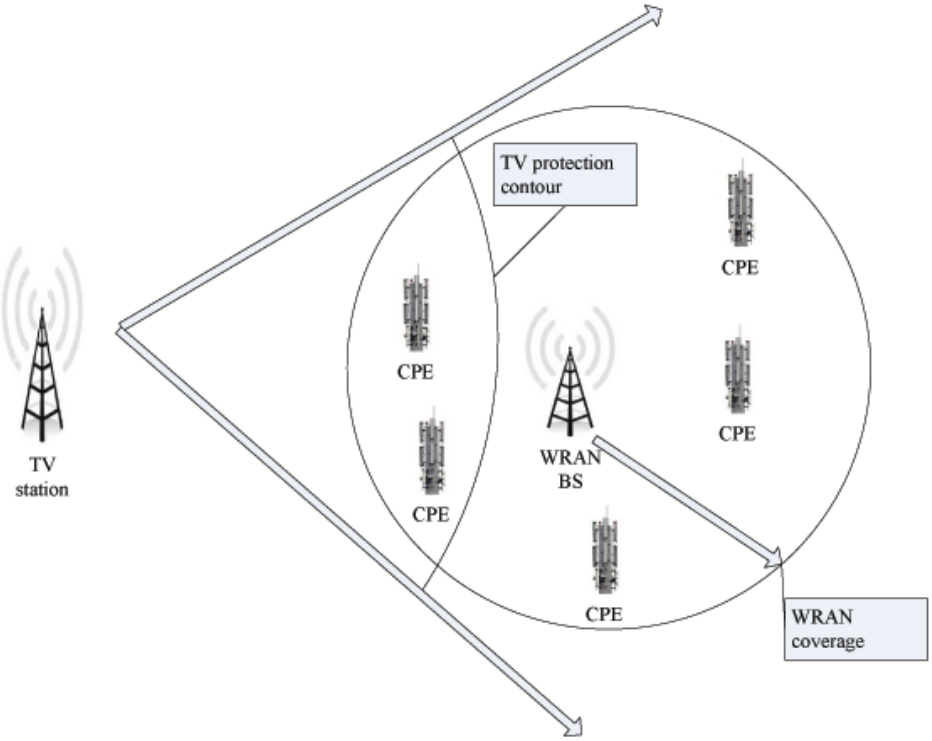

Figure 4.1: The topology of a wireless regional area network (WRAN).

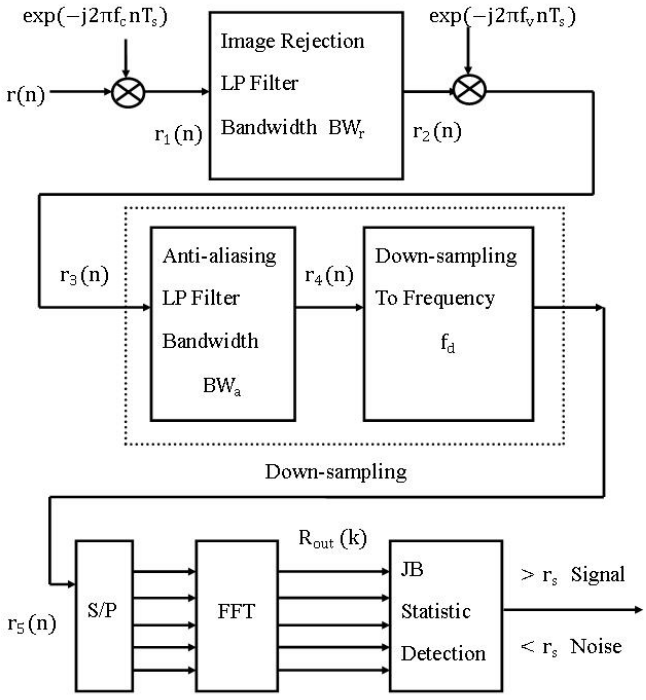

Figure 4.2: The spectrum sensing system diagram.

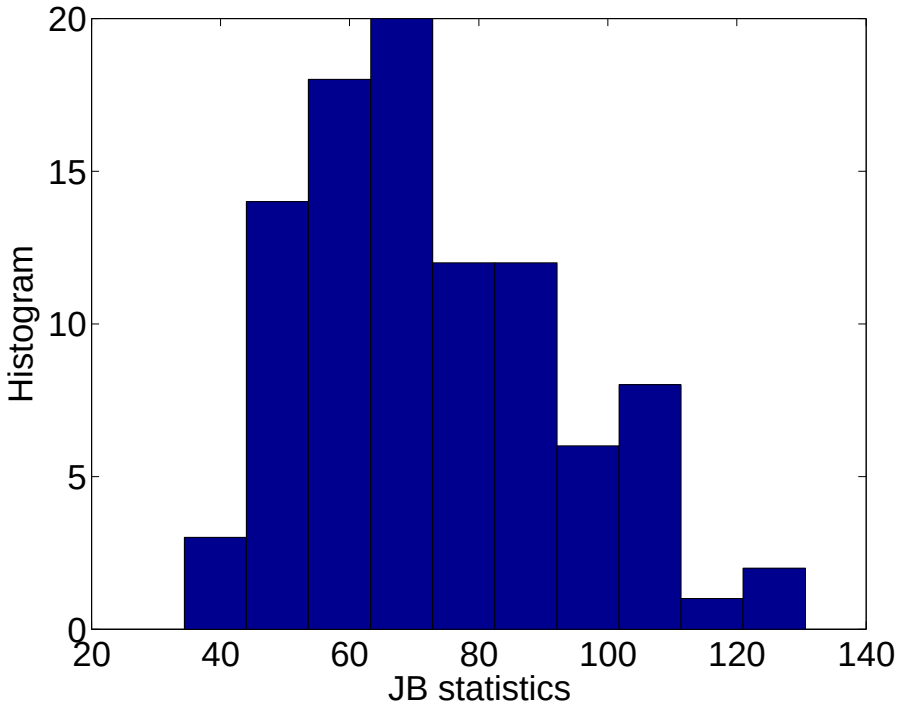

Figure 4.3: A histogram example of the JB statistics.

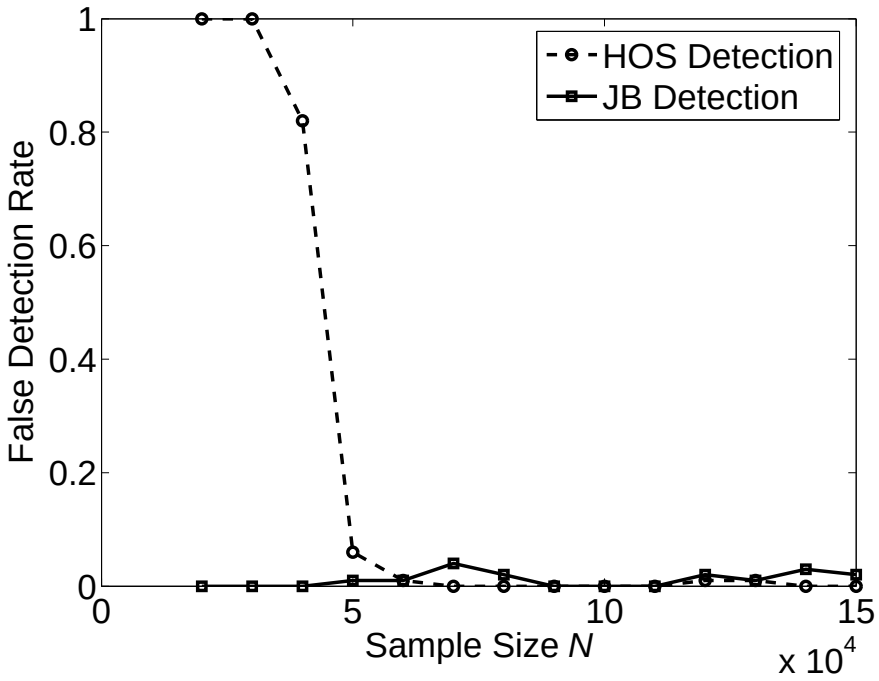

Figure 4.4: False detection rate versus sample size in the sole presence of AWGN.

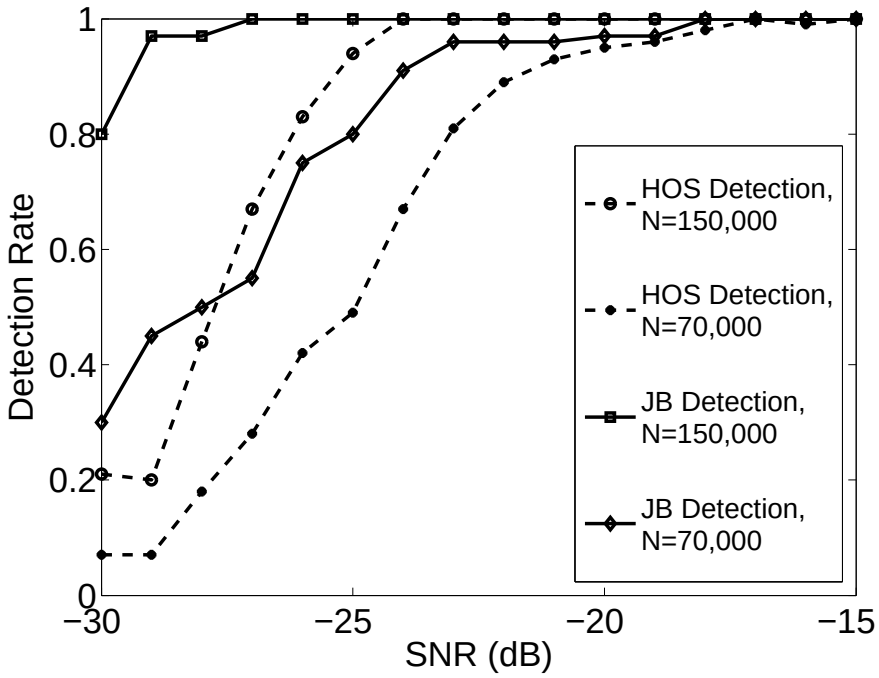

Figure 4.5: Detection rate for simulated wireless microphone signals versus SNR in the single-source case.

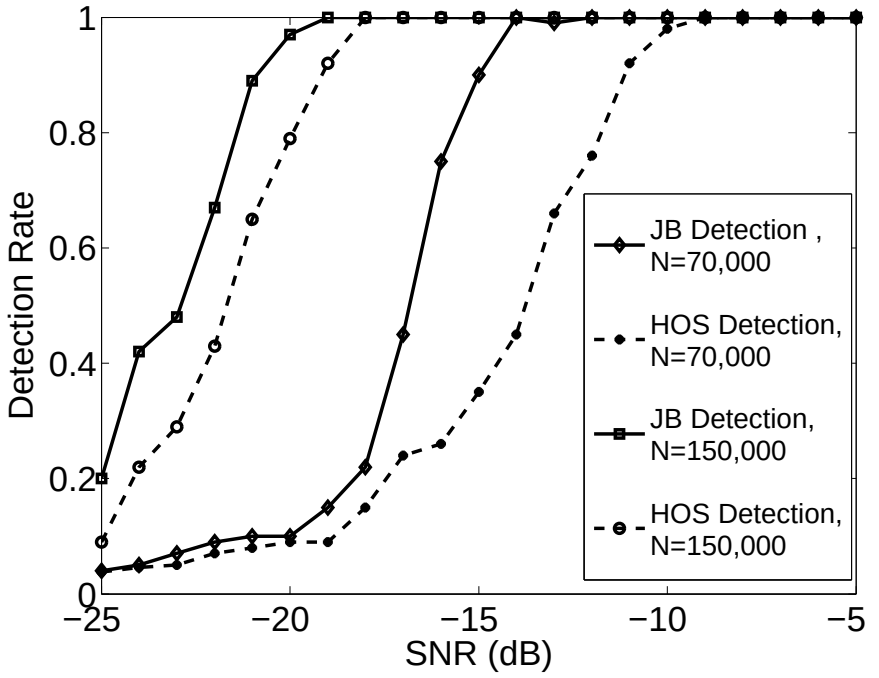

Figure 4.6: Detection rate for real DTV signals versus SNR in the single-source case.

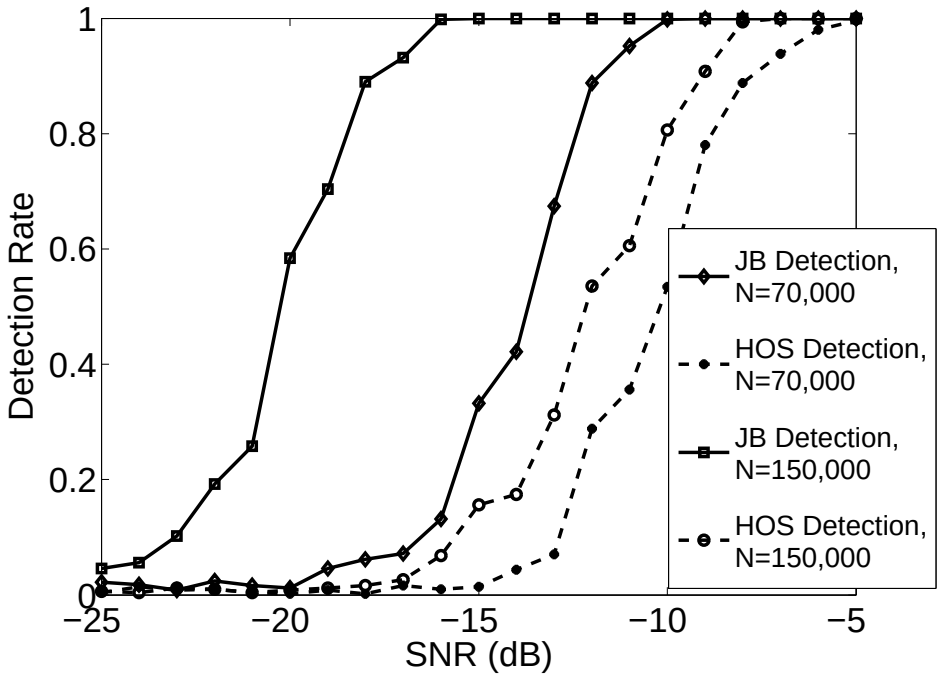

Figure 4.7: Detection rate for real DTV signals versus SNR in the two-source case.

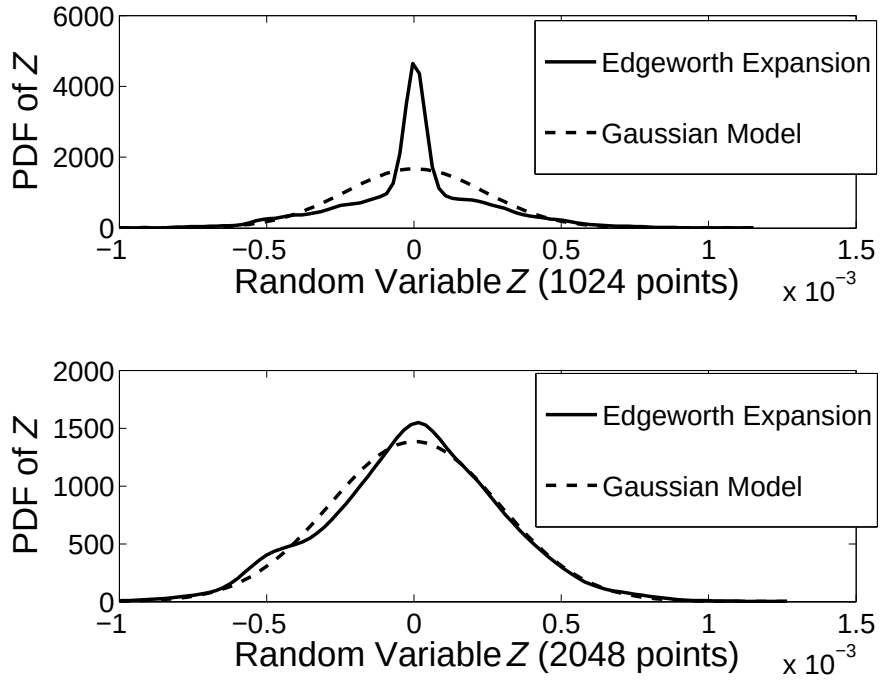

Figure 4.8: The actual PDF resulting from the Edgeworth expansion and the PDF using the underlying Gaussian model for received data ($N = 30,000$, N_{FFT}=2048).

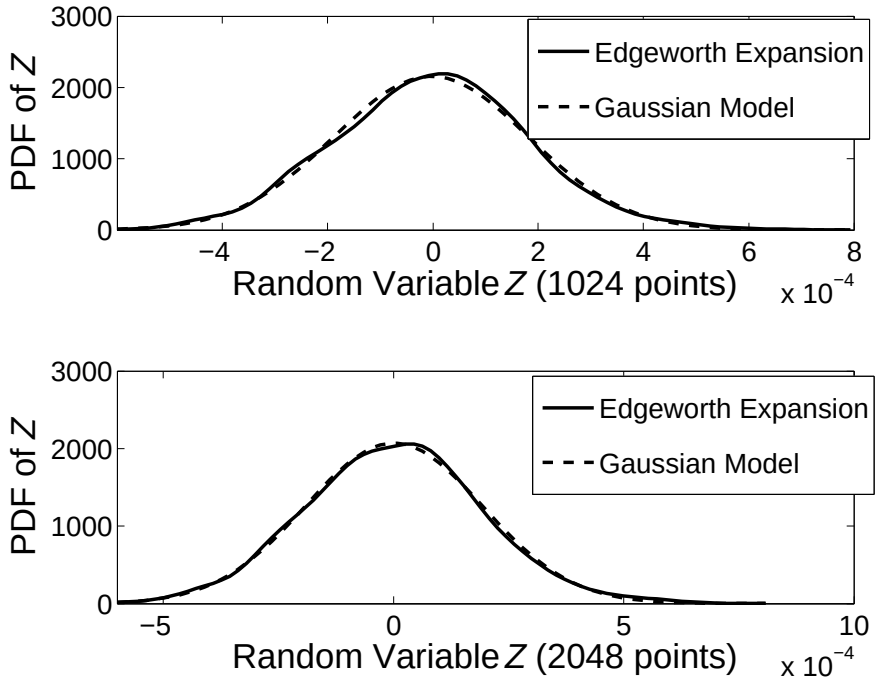

Figure 4.9: The actual PDF resulting from the Edgeworth expansion and the PDF using the underlying Gaussian model for received data ($N = 70,000$, N_{FFT}=2048).

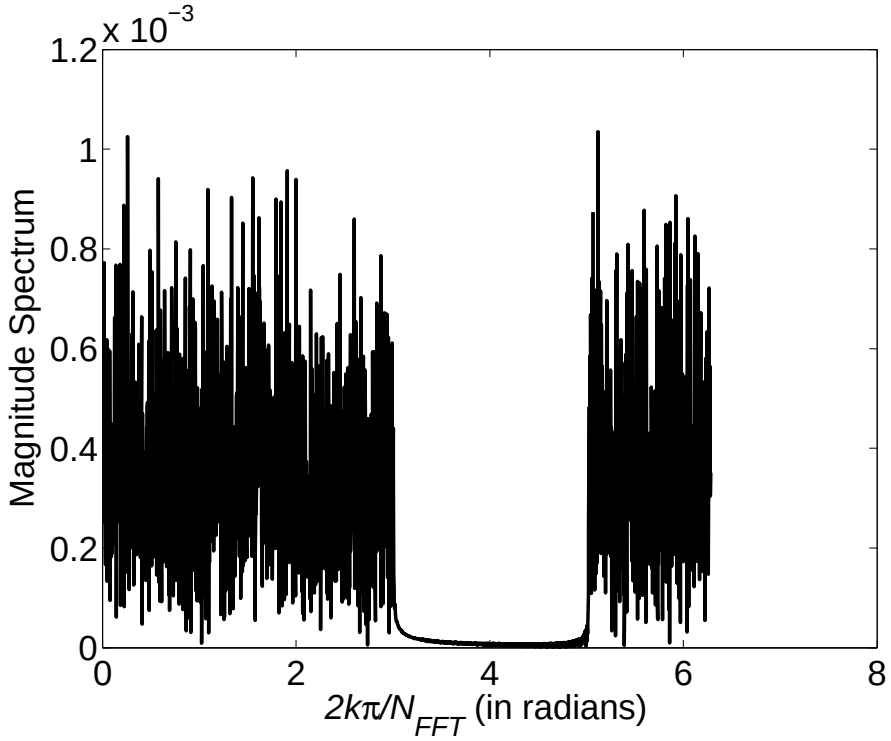

Figure 4.10: $|R_{\text{out}}(k)|$ versus frequency $\frac{2k\pi}{N_{\text{FFT}}}$ ($N = 30,000$).

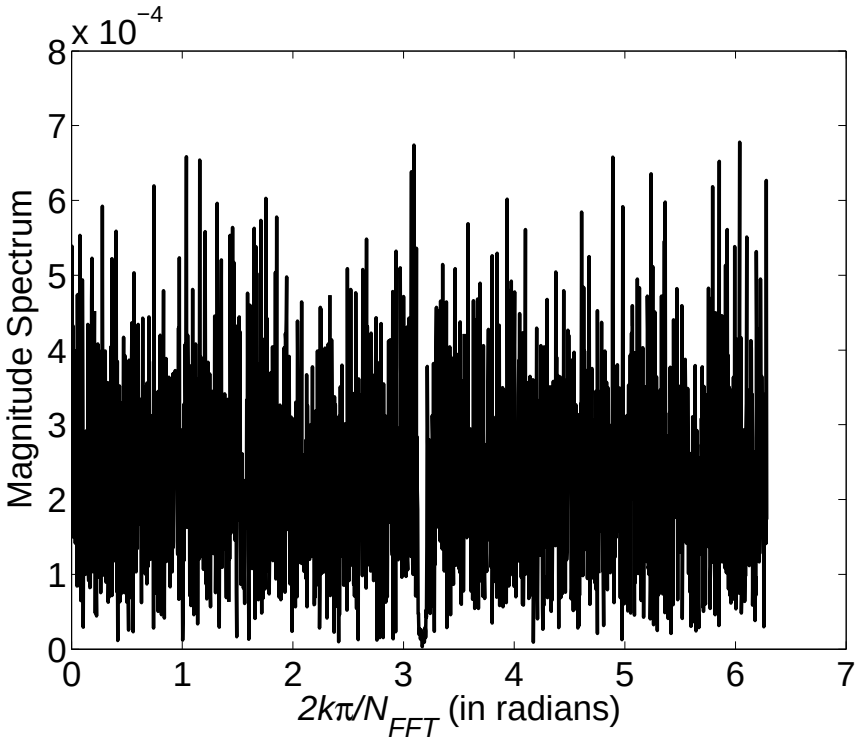

Figure 4.11: $|R_{\text{out}}(k)|$ versus frequency $\frac{2k\pi}{N_{\text{FFT}}}$ $(N = 70,000)$.

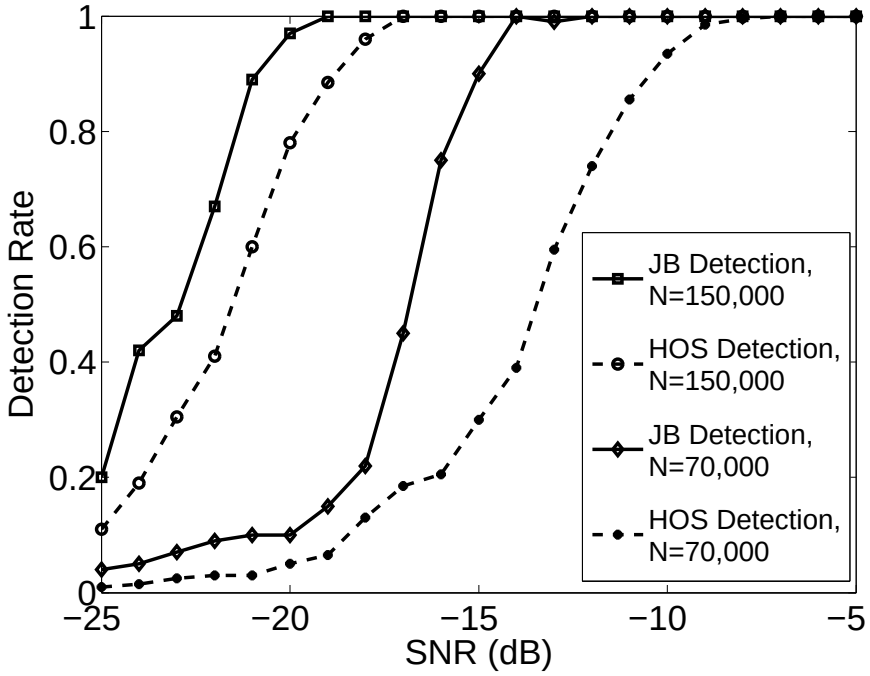

Figure 4.12: Detection rate for real DTV signals versus SNR in the single-source case when the JB detector and the HOS detector are both based on the half-period feature $R_{\text{out}}(k)$, $k = 0, 1, \ldots, \frac{N_{\text{FFT}}}{2} - 1$.

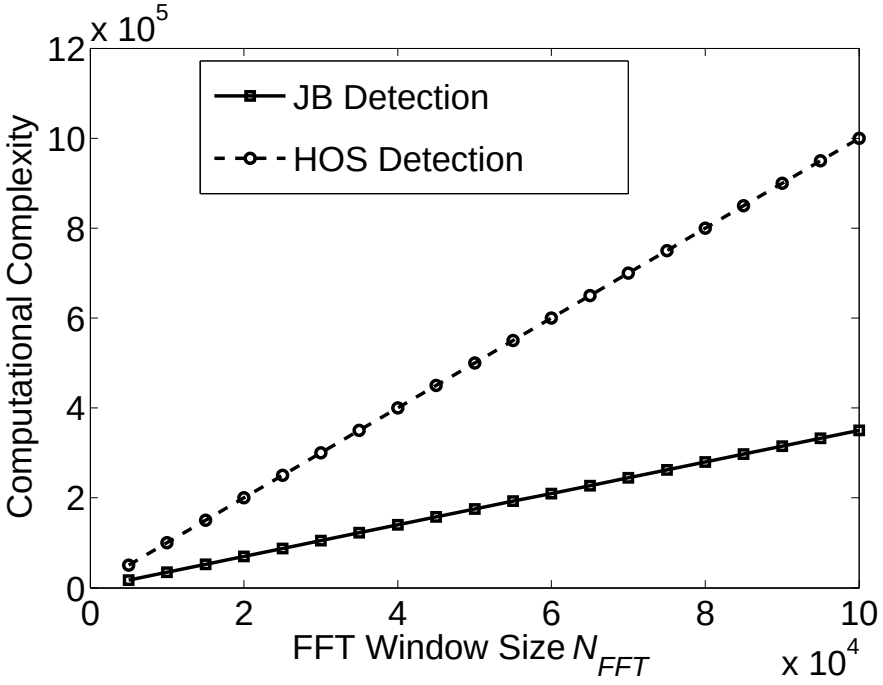

Figure 4.13: Computational complexity measures versus N_{FFT} for our proposed JB detector and the HOS detector.

5. CONCLUSION

In this dissertation work, we investigate some practical signal detection/estimation problems and design new robust and efficient algorithms for communication applications. Three crucial topics are addressed, namely source localization, normality test, and spectrum sensing.

First of all, the source localization problem based on maximal likelihood is simplified by introducing augmented data. We propose a novel EM algorithm which could combat the source localization problem in the presence of spatially non-white Gaussian noise. Compared to the existing SC-ML and AC-ML methods, our algorithm has much better localization accuracy and less computational complexity.

Second, we propose a new normality test, namely the KGGS test, which is quite robust and based on statistics involving both Gaussian and generalized Gaussian PDFs. Our KGGS test can lead to the best test performance compared to other existing normality tests.

Third, we propose a novel spectrum sensing algorithm based on the JB statistic, which is a mathematical combination of skewness and kurtosis. This new method can provide us with much higher detection rate compared with the existing popular HOS detection method. Moreover, our new method can lead to a significant performance margin over the HOS method especially for sparse data. In addition, our new method incurs much less computational complexity than the HOS method.

Besides, we also evaluate the robustness of the aforementioned techniques by different crite-

ria, such as CRLB. These theoretical analyses demonstrate the superiority of our proposed methods to other schemes in terms of performance evaluation and computational complexity. The scientific contributions and findings in this dissertation would be beneficial to the areas of signal processing and wireless communications since robust and efficient techniques are studied and devised for prevalent applications throughout the work.

BIBLIOGRAPHY

[1] W. J. Conover, *Practical Nonparametric Statistics*. Wiley, 1980.

[2] K. Hilal and P. Duhamel, "A blind equalizer allowing soft transition between the constant modulus and the decision-directed algorithm for PSK modulated signals," in *IEEE International Conference on Communications*, vol. 2, pp. 1144–1148, May 1993.

[3] A. Goupil and J. Palicot, "New algorithms for blind equalization: The constant norm algorithm family," *IEEE Transactions on Signal Processing*, vol. 55, pp. 1436–1444, April 2007.

[4] P. Liu and Z. Y. Xu, "Convergence analysis of a new blind equalization algorithm with M-ary PSK channel inputs," in *IEEE International Conference on Acoustics, Speech, and Signal Processing*, vol. 4, pp. 2529–2532, May 2001.

[5] V. Krishnamurthy, S. Dey, and J. P. LeBlanc, "Blind equalization of IIR channels using hidden markov models and extended least squares," *IEEE Transactions on Signal Processing*, vol. 43, pp. 2994–3006, December 1995.

[6] Z. Xu and P. Liu, "New criteria for blind equalization of M-PSK signals," in *Proceedings of 10th IEEE Workshop on Statistical Signal and Array Processing*, pp. 692–696, August 2000.

[7] O. Shalvi and E. Weinstein, "New criteria for blind deconvolution of nonminimum phase systems (channels)," *IEEE Transactions on Information Theory*, vol. 36, pp. 312–321, March 1990.

[8] L. Rota and P. Comon, "Blind equalizers based on polynomial criteria," in *IEEE International Conference on Acoustics, Speech, and Signal Processing*, vol. 4, pp. 441–444, May 2004.

[9] M. Brandstein and D. Ward, *Microphone arrays: Signal Processing Techniques and Applications*. Verlag Berlin Heidelberg New York 2001: Springer, 2001.

[10] S. Makino, T. W. Lee, and H. Sawada, *Signals and Communications Technologys, Blind Speech Seperation*. P.O.BOX 17, 3300AA Dordrecht, The Netherlands.: Springer, 2007.

[11] L. Tong, "Multichannel blind identification: from subspace to maximum likelihood methods," *Proceedings of the IEEE*, vol. 86, pp. 1951–1968, October 1998.

[12] Y. Zhu and K. B. B. Letaief, "Single-carrier frequency-domain equalization with noise prediction for MIMO systems," *IEEE Transactions on Communications*, vol. 55, pp. 1063–1076, May 2007.

[13] P. Tan and N. C. Beaulieu, "A comparison of DCT-based OFDM and DFT-based OFDM in frequency offset and fading channels," *IEEE Transactions on Communications*, vol. 54, pp. 2213–2125, November 2006.

[14] C.-J. Ku and T. L. Fine, "A bayesian independence test for small datasets," *IEEE Transactions on Signal Processing*, vol. 54, pp. 4026–4031, October 2006.

[15] J.-G. Xie and Z.-D. Qiu, "Bootstrap neyman-pearson test for knowing the value of misclassification probability," in *Proceedings of 2005 International Conference on Machine Learning and Cybernetics*, vol. 7, pp. 4394–4399, 2005.

[16] S. Tantaratana and J. Thomas, "Relative efficiency of the sequential probability ratio test in signal detection," *IEEE Transactions on Information Theory*, vol. 24, pp. 22–31, January 1978.

[17] C. Luo, M. Medard, and L. Zheng, "On approaching wideband capacity using multitone FSK," *IEEE Journal on Selected Areas in Communications*, vol. 23, pp. 1830–1838, September 2005.

[18] T. F. Ayoub and A. R. Haimovich, "Modified GLRT signal detection algorithm," *IEEE Transactions on Aerospace and Electronic Systems*, vol. 36, pp. 810–818, July 2000.

[19] F. P. Chitour, J.-P. Y. Ovarlez, P. Forster, and P. Larzabal, "Covariance structure maximum-likelihood estimates in compound gaussian noise: Existence and algorithm analysis," *IEEE Transactions on Signal Processing*, vol. 56, pp. 34–48, January 2008.

[20] M. Honkala, V. Karanko, and J. Roos, "Improving the convergence of combined Newton-Raphson and Gauss-Newton multilevel iteration method," in *IEEE International Symposium on Circuits and Systems*, vol. 2, pp. 229–232, August 2002.

[21] A. P. Dempster, N. M. Laird, and D. B. Rubin, "Maximum likelihood from incomplete data via the EM algorithm," *Journal of the Royal Statistical Society*, vol. 39, no. 1, pp. 1–38, 1977.

[22] M. A. Navakatikyan, C. J. Barrett, G. A. Head, J. H. Ricketts, and S. C. Malpas, "A real-time algorithm for the quantification of blood pressure waveforms," *IEEE Transaction on Biomedical Engineering*, vol. 49, pp. 662–670, July 2002.

[23] H. Krim and M. Viberg, "Two decades of array signal processing research: the parametric approach," *IEEE Signal Processing Magazine*, vol. 13, pp. 67–94, July 1996.

[24] E. F. N. A. Boukerche, H. A. B. Oliveira and A. A. F. Loureiro, "Localization systems for wireless sensor networks," *IEEE Transactions on Wireless Communications*, vol. 6, pp. 6–12, December 2007.

[25] E. Cekli and H. A. Cirpan, "Unconditional maximum likelihood approach for localization of near-field sources: Algorithm and performance analysis," *AEU International Journal of Electronics and Communications*, vol. 57, pp. 9–15, January 2003.

[26] K. Afkhamie and Z.-Q. Luo, "Blind identification of FIR systems driven by markov-like input signals," *IEEE Transactions on Signal Processing*, vol. 48, pp. 1726–1736, June 2000.

[27] H. Zamiri-Jafarian and S. Pasupathy, "Adaptive MLSDE using the EM algorithm," *IEEE Transactions on Communications*, vol. 47, pp. 1181–1193, August 1999.

[28] Y. Zhao, "An EM algorithm for linear distortion channel estimation based on observations from a mixture of gaussian sources," *IEEE Transactions on Speech and Audio Processing*, vol. 7, pp. 400–413, July 1999.

[29] A. Al-Smadi, "Fitting ARMA models to linear non-Gaussian processes using higher order statistics," *Signal Processing*, vol. 82, pp. 1789–1793, November 2002.

[30] E. P. Tsolaki, "Testing nonstationary time series for Gaussianity and linearity using the evolutionary bispectrum: An application to internet traffic data," *Signal Processing*, vol. 10, pp. 1355–1567, June 2008.

[31] D. Stopler and R. Zamir, "Capacity and error probability in single-tone and multitone multiple access over an impulsive channel," *IEEE Transactions on Communications*, vol. 49, pp. 506–517, March 2001.

[32] V. Weerackody, S. A. Kassam, and K. R. Laker, "Convergence analysis of an algorithm for blind equalization," *IEEE Transactions on Communications*, vol. 39, pp. 856–865, June 1991.

[33] Z. Tang and W. E. Ryan, "Achievable information rates and the coding-spreading tradeoff in finite-sized synchronous CDMA systems," *IEEE Transactions on Communications*, vol. 53, pp. 1432–1437, September 2005.

[34] D. Cabric, A. Tkachenko, and R. W. Brodersen, "Spectrum sensing measurements of pilot, energy, and collaborative detection," in *Proceedings of IEEE Military Communications Conference*, pp. 1–7, October 2006.

[35] Y.-C. Liang, H.-H. Chen, J. Mitola, P. Mahonen, R. Kohno, J. H. Reed, and L. Milstein, "Guest editorial - cognitive radio: Theory and application," *IEEE Journal on Selected Areas in Communications*, vol. 26, pp. 1–4, May 2008.

[36] L. Zhang, Y.-C. Liang, and Y. Xin, "Joint beamforming and power allocation for multiple access channels in cognitive radio networks," *IEEE Journal on Selected Areas in Communications*, vol. 26, pp. 38–51, January 2008.

[37] Y. H. Zeng and Y.-C. Liang, "Eigenvalue based spectrum sensing algorithms for cognitive radio," *IEEE Transactions on Communications*, vol. 57, pp. 1784–1793, June 2009.

[38] T. Yucek and H. Arslan, "A survey of spectrum sensing algorithms for cognitive radio applications," *IEEE Communications Surveys and Tutorials*, vol. 11, pp. 116–130, March 2009.

[39] L. Ljung, *System Identification*. Prentice-Hall, New Jersey, 1999.

[40] K. E. Hild, H. T. Attias, and S. S. Nagarajan, "An expectation-maximization method for spatio-temporal blind source separation using an AR-MOG source model," *IEEE Transactions on Neural Networks*, vol. 19, pp. 508–519, March 2008.

[41] V. P. Tuzlukov, *Signal Detection Theory*. Birkhauser, 2001.

[42] A. N. Shiryayev, *Selected Works of A.N. Kolmogorov: vol. 2 Probability Theory and Mathematical Statistics*. Springer, 1992.

[43] N. Wiener, *Extrapolation, Interpolation, and Smoothing of Stationary Time Series with Engineering Applications Application: With Engineering Applications*. Mit Press, 1964.

[44] J. I. Marcum, *A Statistical Theory of Target Detection by Pulsed Rada*. RAND Corporation, 1947.

[45] J. A. Swets, *Signal detection and recognition by human observers*. Wiley, 1964.

[46] E. B. Manoukian, *Modern Concepts and Theorems of Mathematical Statistics*. Springer, 1986.

[47] R. O. Duda, P. E. Hart, and D. G. Stork, *Pattern Classification, Second Edition*. 605 Third Avenue, New York: Wiley and Sons, Inc., 2001.

[48] E. B. Manoukian, *Modern Concepts and Theorems of Mathematical Statistics*. Springer, 1986.

[49] J. C. Chen, R. E. Hudson, and K. Yao, "Maximum-likelihood source localization and unknown sensor location estimation for wideband signals in the near-field," *IEEE Transactions on Signal Processing*, vol. 50, pp. 1843–1854, August 2002.

[50] J. C. Chen, R. E. Hudson, and K. Yao, "Source localization of a wideband source using a randomly distributed beamforming sensor array," in *Proceedings of International Society of Information Fusion*, pp. TuC1: 11–18, 2001.

[51] P. Stoica and A. Nehorai, "Music, maximum likelihood and Cramer-Rao bound," *IEEE Transactions on Acoustics, Speech and Signal Processing*, vol. 37, pp. 720–741, May 1989.

[52] P. Stoica and A. Nehorai, "Performance study of conditional and unconditional direction-of-arrival estimation," *IEEE Transactions on Acoustics, Speech, and Signal Processing*, vol. 38, no. 10, pp. 1783–1795, 1990.

[53] C. E. Chen, F. Lorenzelli, R. E. Hudson, and K. Yao, "Maximum likelihood DOA estimation of multiple wideband sources in the presence of nonuniform sensor noise," *EURASIP Journal on Advances in Signal Processing*, vol. 2008, 2008.

[54] M. Pesavento and A. B. Gershman, "Maximum-likelihood direction-of-arrival estimation in the presence of unknown nonuniform noise," *IEEE Transactions on Signal Processing*, vol. 49, no. 7, pp. 1310–1324, 2001.

[55] E. B. Manoukian, *Modern Concepts and Theorems of Mathematical Statistics*. Springer, 1986.

[56] S. S. Shapiro, M. B. Wilk, and H. J. Chen, "A comparative study of various tests of normality," *Journal of the American Statistical Association*, vol. 63, pp. 1343–1372, 1968.

[57] E. S. Pearson, R. B. D'Agostino, and K. O. Bowman, "Tests for departure from normality: comparison of powers," *Biometrika*, vol. 64, no. 2, pp. 231–246, 1977.

[58] H. Lilliefors, "On the Kolmogorov-Smirnov test for normality with mean and variance unknown," *Journal of the American Statistical Association*, vol. 62, pp. 399–402, June 1967.

[59] C. M. Jarque and A. K. Bera, "Efficient tests for normality, homoscedasticity and serial independence of regression residuals," *Economics Letters*, vol. 7, no. 4, pp. 313–318, 1981.

[60] A. M. Zoubir and M. J. Arnold, "Testing Gaussianity with the characteristic function: The i.i.d. case," *Signal Processing*, vol. 53, no. 2-3, pp. 245–255, 1996.

[61] E. Moulines, J. M. D. Molle, K. Choukri, and M. Charbit, "Testing that a stationary time-series is Gaussian: time-domain vs. frequency-domain approaches," in *Proceedings of IEEE Signal Processing Workshop on Higher-Order Statistics*, pp. 336–340, June 1993.

[62] J. W. D. Molle and M. J. Hinich, "Trispectral analysis of stationary random time series," *The Journal of the Acoustical Society of America*, vol. 97, pp. 2963–2978, May 1995.

[63] A. Sahai and D. Cabric, "Spectrum sensing: fundamental limits and practical challenges," in *IEEE International Symposium on New Frontiers Dynamic Spectrum Access Networks*, November 2005.

[64] H. S. Chen, W. Gao, and D. G. Daut, "Signature based spectrum sensing algorithms for IEEE 802.22 WRAN," in *Proceedings of IEEE International Conference on Communications (ICC)*, pp. 6487–6492, June 2007.

[65] S. Enserink and D. Cochran, "A cyclostationary feature detector," in *Proceedings of Asilomar Conference on Signals, Systems and Computers*, vol. 2, pp. 806–810, October-November 1994.

[66] Y. P. Lin and C. He, "Subsection-average cyclostationary feature detection in cognitive radio," in *Proceedings of International Conference on Neural Networks and Signal Processing*, pp. 604–608, July 2008.

[67] S. M. Kay, *Fundamentals of Statistical Signal Processing: Detection Theory*. Upper Saddle River, New Jersey: Prentice-Hall, 1998.

[68] S. J. Shellhammer, S. Shankar, R. Tandra, and J. Tomcik, "Performance of power detector sensors of DTV signals in IEEE 802.22 WRANs," in *Proceedings of the Fist International Workshop on Technology and Policy for Accessing Spectrum (TAPAS)*, August 2006.

[69] A. Sonnenschein and P. M. Fishman, "Radiometric detection of spreadspectrum signals in noise of uncertainty power," *IEEE Transactions on Aerospace and Electronic Systems*, vol. 28, pp. 654–660, July 1992.

[70] R. Tandra and A. Sahai, "Fundamental limits on detection in low SNR under noise uncertainty," in *Proceedings of International Conference on Wireless Networks, Communications and Mobile Computing*, vol. 1, pp. 464–469, June 2005.

[71] H. Urkowitz, "Energy detection of unknown deterministic signals," *Proceedings of the IEEE*, vol. 55, pp. 523–531, April 1967.

[72] Y.-C. Liang, Y. H. Zeng, E. C. Y. Peh, and A. T. Hoang, "Sensing-throughput tradeoff for cognitive radio networks," *IEEE Transactions on Wireless Communication*, vol. 7, pp. 1326–1337, April 2008.

[73] A. N. Mody, "Spectrum sensing of the DTV in the vicinity of the video carrier using higher order statistics," July 2007.

[74] K. Yan, H.-C. Wu, and S. S. Iyengar, "Robustness analysis of source localization using Gaussianity measure," in *Proceedings of IEEE Global Telecommunications Conference*, pp. 1–5, November 2008.

[75] K. K. Mada and H.-C. Wu, "EM algorithm for multiple wideband source," *in Proceedings of IEEE Global Telecommunications Conference*, pp. 1–5, 2006.

[76] K. K. Mada, H.-C. Wu, and S. S. Iyengar, "Efficient and robust EM algorithm for multiple wideband source localization," *IEEE Transactions on Vehicular Technology*, vol. 58, pp. 3071–3075, July 2009.

[77] F. F. Digham, M. S. Alouini, and M. K. Simon, "On the energy detection of unknown signals over fading channels," *IEEE Transactions on Communications*, vol. 55, pp. 21–24, January 2007.

[78] S. Niranjayan and N. C. Beaulieu, "The BER optimal linear rake receiver for signal detection in symmetric alpha-stable noise," *IEEE Transactions on Communications*, vol. 57, pp. 3585–3588, December 2009.

[79] M. N. Do and M. Vetterli, "Wavelet-based texture retrieval using generalized Gaussian density and Kullback-Leibler distance," *IEEE Transactions on Image Processing*, vol. 11, pp. 238–240, February 2002.

[80] D. H. Johnson and G. C. Orsak, "Relation of signal set choice to the performance of optimal non-Gaussian detectors," *IEEE Transactions on Communications*, vol. 41, pp. 1319–1328, September 1993.

[81] "Initial signal processing of captured DTV signals for evaluation of detection algorithms," August 2006.

[82] C. L. Nikias and A. P. Petropulu, *Higher-Order Spectra Analysis*. New Jersey: Prentice-Hall, 1993.

[83] "Wikipedia webpage on Rayleigh distribution," 2010.

[84] C. Clanton, M. Kenkel, and Y. Tang, "Wireless microphone signal simulation method," March 2007.

[85] S. Shellhammer, "Numerical spectrum sensing requirements," June 2006.

[86] S. Shellhammer, V. Tawil, G. Chouinard, M. Muterspaugh, and M. Ghosh, "Spectrum sensing simulation model," March 2006.

[87] A. Renaux, P. Forster, P. Larzabal, and E. Boyer, "Unconditional maximum likelihood performance at finite number of samples and high signal-to-noise ratio," *IEEE Transactions on Signal Processing*, vol. 55, pp. 2258–2364, May 2007.

[88] N. Menemenlis and C. D. Charalambous, "An Edgeworth series expansion for multipath fading channel densities," in *Proceedings of IEEE Conference on Decision and Control*, vol. 4, pp. 4030–4035, December 2002.

[89] H. Cramer, *Random Variables and Probability Distributions*. Cambridge University Press, 1970.

APPENDIX: LETTER OF PERMISSION

From: Jacqueline Hansson Date: 07/22/2011

Subject: Re: Request for Send To: llu4@tigers.lsu.edu Permission.

Dear Lu Lu :

In response to your email below, we are happy to grant you this permission to reprint your below described IEEE copyrighted papers in your thesis and, if you wish, have your paper placed on your universitys website. These are IEEE's requirements:

(1) The following IEEE copyright/credit notice must be placed prominently on the first page of the reprinted material, with the appropriate details filled in: © [year of original publication] IEEE. Reprinted, with permission, from [author names, paper title, IEEE publication title, and month/year of publication].

(2) The following message should be displayed at the beginning of the credits or in an appropriate place on the website: This material is posted here with permission of the IEEE. Such permission of the IEEE does not in any way imply IEEE endorsement of any of Louisiana State University's products or services. Internal or personal use of this material is permitted. However, permission to reprint/republish this material for advertising or promotional purposes or for creating new collective works for resale or redistribution must be obtained from the IEEE by writing to pubs-permissions@ieee.org .By choosing to view this material, you agree to all provisions of the copyright laws protecting it.

If applicable, University Microfilms, Inc. and/or ProQuest may supply single copies of the dissertation.

For your future requests for IEEE copyrighted material, IEEE is pleased to announce our partnership with Copyright Clearance Centers RightsLink service. RightsLink offers a fast and easy way to obtain permission to reuse and republish material from IEEE. In the future, please follow these simple instructions to obtain permission through RightsLink. (1) Please use the IEEE Xplore Search function to find the title of the IEEE copyrighted paper you're req uesting to use, (2) click on the IEEE paper title (3) Next, click on the Rights and Permissions link (4) Create your RightsLink account, select your reuse preferences and obtain permission for the IEEE content you have requested.

If you have any further questions, or if we can be of additional assistance, please do not hesitate to contact me

Sincerely,

Jacqueline Hansson, Coordinator

IEEE Intellectual Property Rights Office 445 Hoes Lane Piscataway, NJ 08855-1331 USA +1 732 562 3966 (phone) +1 732 562 1746 (fax)

IEEE– Fostering technological innovation and excellence for the benefit of humanity.

==========

Dear Sir or Madam,

This is Lu Lu from Louisiana State University. I sincerely would like to ask for your permission to reprint the following articles accepted and published by IEEE journals:

Paper 1 Author(s) : Lu Lu, Hsiao-Chun Wu, Kun Yan, and Iyengar, S.S.;

Paper Title: Robust Expectation-Maximization Algorithm for Multiple Wideband Acoustic

Source Localization in the Presence of Nonuniform Noise Variances

IEEE publication title: IEEE Sensors Journal

Paper 2 Author(s) : Lu Lu, Hsiao-Chun Wu and S.S. Iyengar,

Paper Title: A Novel Robust Detection Algorithm for Spectrum Sensing

IEEE publication title: IEEE Transactions on Selected Areas in Communications

As one of the authors of these papers, I want to reprint the entire articles as Chapter 2 and Chapter 4 in my dissertation with the tile Efficient and Robust Signal Detection Algorithms for The Communication Applications. The requested permission extends to any future revisions and editions of my dissertation, and the dissertation will be put in the electronic thesis and dissertation library of Louisiana State University. These rights will in no way restrict republication of the materials in any other form by IEEE or by others authorized by IEEE. Your permission of this request will also confirm that IEEE owns the copyright of the above-described materials.

If these arrangements meet with your approval, I will greatly appreciate that you could response this email no later than Monday July 25th, 2011. Thank you so much for your cooperation.

Sincerely, Lu Lu

VITA

Lu Lu received a Bachelor Engineering degree from Taiyuan University of Science and Technology Electrical Engineering Department in 2005. He got a Master of Engineering degree from Xi'an Jiaotong University in 2008. He is currently pursuing the degree of Doctor of Philosophy in the Department Electrical and Computer Engineering Department, Louisiana State University, Baton Rouge. His research interests are in the areas of wireless communications and signal processing.

Lu, Lu B.S. Electrical Engineering, Taiyuan University of Science and Technology, 2005
M.S. Electrical Engineering, Xi'an Jiaotong University, 2008
Doctor of Philosophy, Fall Commencement, 2011
Major: Electrical Engineering
Efficient and Robust Signal Detection Algorithms for the Communication Applications
Dissertation directed by Associate Professor Hsiao-Chun Wu
Pages in dissertation, 100. Words in abstract, 209.

ABSTRACT

Signal detection and estimation has been prevalent in signal processing and communications for many years. The relevant studies deal with the processing of information-bearing signals for the purpose of information extraction. Nevertheless, new robust and efficient signal detection and estimation techniques are still in demand since there emerge more and more practical applications which rely on them. In this dissertation work, we proposed several novel signal detection schemes for wireless communications applications, such as *source localization algorithm*, *spectrum sensing method*, and *normality test*. The associated theories and practice in *robustness*, *computational complexity*, and *overall system performance evaluation* are also provided.